Soluble organic molecules in samples of the carbonaceous asteroid (162173) Ryugu

Hiroshi Naraoka[1]*, Yoshinori Takano[2], Jason P. Dworkin[3], Yasuhiro Oba[4], Kenji Hamase[5], Aogu Furusho[5#], Nanako O. Ogawa[2], Minako Hashiguchi[6], Kazuhiko Fukushima[7], Dan Aoki[7], Philippe Schmitt-Kopplin[8,9,10], José C. Aponte[3], Eric T. Parker[3], Daniel P. Glavin[3], Hannah L. McLain[3,11,12], Jamie E. Elsila[3], Heather V. Graham[3], John M. Eiler[13], Francois-Regis Orthous-Daunay[14], Cédric Wolters[14], Junko Isa[15,16], Véronique Vuitton[14], Roland Thissen[17], Saburo Sakai[2], Toshihiro Yoshimura[2], Toshiki Koga[2], Naohiko Ohkouchi[2], Yoshito Chikaraishi[4], Haruna Sugahara[18], Hajime Mita[19], Yoshihiro Furukawa[20], Norbert Hertkorn[8], Alexander Ruf[21,22,23], Hisayoshi Yurimoto[24], Tomoki Nakamura[20], Takaaki Noguchi[25], Ryuji Okazaki[1], Hikaru Yabuta[26], Kanako Sakamoto[18], Shogo Tachibana[18,27], Harold C. Connolly, Jr.[28], Dante S. Lauretta[29], Masanao Abe[18,30], Toru Yada[18], Masahiro Nishimura[18], Kasumi Yogata[18], Aiko Nakato[18], Miwa Yoshitake[18], Ayako Suzuki[31], Akiko Miyazaki[18], Shizuho Furuya[27], Kentaro Hatakeda[31], Hiromichi Soejima[31], Yuya Hitomi[31], Kazuya Kumagai[31], Tomohiro Usui[18], Tasuku Hayashi[18], Daiki Yamamoto[18], Ryota Fukai[18], Kohei Kitazato[32], Seiji Sugita[16,27], Noriyuki Namiki[30,33], Masahiko Arakawa[34], Hitoshi Ikeda[18], Masateru Ishiguro[35], Naru Hirata[31], Koji Wada[16], Yoshiaki Ishihara[36], Rina Noguchi[37], Tomokatsu Morota[27], Naoya Sakatani[38], Koji Matsumoto[30,33], Hiroki Senshu[16], Rie Honda[38], Eri Tatsumi[39], Yasuhiro Yokota[18], Chikatoshi Honda[32], Tatsuhiro Michikami[40], Moe Matsuoka[18]§, Akira Miura[18], Hirotomo Noda[30,33], Tetsuya Yamada[18], Keisuke Yoshihara[18], Kosuke Kawahara[18], Masanobu Ozaki[18,30], Yu-ichi Iijima[18]†, Hajime Yano[18,30], Masahiko Hayakawa[18], Takahiro Iwata[18], Ryudo Tsukizaki[18], Hirotaka Sawada[18], Satoshi Hosoda[18], Kazunori Ogawa[42], Chisato Okamoto[34]†, Naoyuki Hirata[33], Kei Shirai[33], Yuri Shimaki[18], Manabu Yamada[16], Tatsuaki Okada[18,43], Yukio Yamamoto[18,30], Hiroshi Takeuchi[18,30], Atsushi Fujii[18], Yuto Takei[18], Kento Yoshikawa[36], Yuya Mimasu[18], Go Ono[36], Naoko Ogawa[18], Shota Kikuchi[16,33], Satoru Nakazawa[18], Fuyuto Terui[44], Satoshi Tanaka[18,30], Takanao Saiki[18], Makoto Yoshikawa[18,30], Sei-ichiro Watanabe[6] and Yuichi Tsuda[18]

[1]Department of Earth and Planetary Sciences, Kyushu University, Fukuoka 819-0395, Japan.

[2]Biogeochemistry Research Center, Japan Agency for Marine-Earth Science and Technology, Yokosuka 237-0061, Japan.

[3]Solar System Exploration Division, NASA Goddard Space Flight Center, Greenbelt, MD 20771, USA.

[4]Institute of Low Temperature Sciences, Hokkaido University, Sapporo 060-0189, Japan.

[5]Graduate School of Pharmaceutical Sciences, Kyushu University, Fukuoka 812-8582, Japan.

[6]Graduate School of Environment Studies, Nagoya University, Nagoya 464-8601, Japan.

[7]Graduate School of Bioagricultural Sciences, Nagoya University, Nagoya 464-8601, Japan.

[8]Helmholtz Munich, Analytical BioGeoChemistry, Neuherberg 85764, Germany.

[9]Technische Universität München, Analytische Lebensmittel Chemie, Freising 85354, Germany.

[10]Max Planck Institute for Extraterrestrial Physics, Garching bei München 85748, Germany.

[11]Center for Research and Exploration in Space Science and Technology, NASA Goddard Space Flight Center, Greenbelt, MD 20771, USA.

[12]Department of Physics, The Catholic University of America, Washington, D.C. 20064, USA.

[13]Division of Geological and Planetary Sciences, California Institute of Technology, Pasadena, CA 91125, USA.

[14]Université Grenoble Alpes, Centre National de la Recherche Scientifique (CNRS), Centre National d'Etudes Spatiales, L'Institut de Planétologie et d'Astrophysique de Grenoble, Grenoble 38000, France.

[15]Earth-Life Science Institute, Tokyo Institute of Technology, Tokyo 152-8550, Japan.

[16]Planetary Exploration Research Center, Chiba Institute of Technology, Narashino 275-0016, Japan.

[17]Université Paris-Saclay, CNRS, Institut de Chimie Physique, Orsay 91405, France.

[18]Institute of Space and Astronautical Science, Japan Aerospace Exploration Agency (JAXA), Sagamihara 252-5210, Japan.

[19]Department of Life, Environment and Material Science, Fukuoka Institute of Technology, Fukuoka 811-0295, Japan.

[20]Department of Earth Science, Tohoku University, Sendai 980-8578, Japan.

[21]Université Aix-Marseille, CNRS, Laboratoire de Physique des Interactions Ioniques et Moléculaires, Marseille 13397, France.

[22]Department of Chemistry and Pharmacy, Ludwig-Maximilians-University, Munich 81377, Germany.

[23]Excellence Cluster ORIGINS, Garching 85748, Germany.

[24]Department of Earth and Planetary Sciences, Hokkaido University, Sapporo 060-0810, Japan.

[25]Division of Earth and Planetary Sciences, Kyoto University, Kyoto 606-8502, Japan.

[26]Department of Earth and Planetary Systems Science, Hiroshima University, Higashi-Hiroshima 739-8526, Japan.

[27]Department of Earth and Planetary Science, University of Tokyo, Tokyo 113-0033, Japan.

[28]Department of Geology, School of Earth and Environment, Rowan University, Glassboro, NJ 08028, USA.

[29]Lunar and Planetary Laboratory, University of Arizona, Tucson, AZ 85721, USA.

[30]School of Physical Sciences, The Graduate University for Advanced Studies, Hayama 240-0193, Japan.

[31]Marine Works Japan Ltd., Yokosuka 237-0063, Japan.

[32]Aizu Research Cluster for Space Science, University of Aizu, Aizu-Wakamatsu 965-8580, Japan.

[33]Research of Interior Structure and Evolution of Solar System Bodies, National Astronomical Observatory of Japan, Mitaka 181-8588, Japan.

[34]Department of Planetology, Kobe University, Kobe 657-8501, Japan.

[35]Department of Physics and Astronomy, Seoul National University, Seoul 08826, Republic of Korea.

[36]Research and Development Directorate, JAXA, Sagamihara 252-5210, Japan.

[37]Faculty of Science, Niigata University, Niigata 950-2181, Japan.

[38]Department of Physics, Rikkyo University, Tokyo 171-8501, Japan.

[39]Center of Data Science, Ehime University, Matsuyama 790-8577, Japan.

[40]Instituto de Astrofísica de Canarias, University of La Laguna, Tenerife E-38205, Spain.

[41]Faculty of Engineering, Kindai University, Higashi-Hiroshima 739-2116, Japan.

[42]JAXA Space Exploration Center, JAXA, Sagamihara 252-5210, Japan.

[43]Department of Chemistry, University of Tokyo, Tokyo 113-0033, Japan.

[44]Departmen of Mechanical Engineering, Kanagawa Institute of Technology, Atsugi 243-0292, Japan.

*Corresponding author. Email: naraoka@geo.kyushu-u.ac.jp

†Deceased.

#Present address: School of Pharmaceutical Sciences, University of Shizuoka, Shizuoka 422-8526, Japan.

§Present address: Geological Survey of Japan, National Institute of Advanced Industrial Science and Technology, Tsukuba 305-8567, Japan.

The Hayabusa2 spacecraft collected samples from the surface of the carbonaceous near-Earth asteroid (162173) Ryugu, and brought them to Earth. The samples were expected to contain organic molecules, which record processes that occurred in the early Solar System. We analyzed organic molecules extracted from the Ryugu surface samples. We identify a variety of molecules containing the atoms CHNOS, formed by methylation, hydration, hydroxylation, and sulfurization reactions. Amino acids, aliphatic amines, carboxylic acids, polycyclic aromatic hydrocarbons, and nitrogen-heterocyclic compounds were detected, with properties consistent with an abiotic origin. These compounds likely arose from aqueous reaction on Ryugu's parent body and are similar to organics in Ivuna-type meteorites. These molecules can survive on the surfaces of asteroids and be transported throughout the Solar System.

A variety of organic molecules have been identified in carbonaceous chondrite meteorites, especially the meteorite types that experienced aqueous alteration (reactions with liquid water). Prebiotic molecules, such as amino acids, have been found in meteorite soluble organic matter (SOM) (*1*), suggesting that they could have been delivered to the early Earth (*2, 3*). It is unclear

which Solar System objects are the parent bodies of carbonaceous chondrites (*4*). Carbonaceous (C-type) asteroids, common in the asteroid belt, have been hypothesized as possible parent bodies of carbonaceous chondrites, based on spectroscopic similarities (*5*).

The Hayabusa2 spacecraft investigated the near-Earth C-type asteroid (162173) Ryugu. Ryugu has a low-albedo surface, consisting of hydrous minerals and carbonaceous materials (*6*). Hayabusa2 collected ~5 grams of samples from Ryugu's surface and delivered them to Earth on 2020 December 6 (*7*). Unlike meteorites, these samples were collected from a specific spot on the surface of a well-characterized asteroid and retrieved without contamination from the biosphere. We analyzed Ryugu samples to characterize their SOM contents, with the goal of determining the evolutionary history of these organic compounds. Organics could have formed and/or been modified by chemical processes in the molecular cloud from which the Solar System formed, in the proto-solar nebula during the process of planet formation, or on the planetesimal that became the parent body of Ryugu. Because the surface of Ryugu is exposed to the vacuum of space, irradiation by energetic particles (cosmic rays), heating by sunlight and micrometeoroid impacts, could all have altered the SOM.

Ryugu samples investigated for SOM

All Ryugu samples are dominated by hydrous silicate minerals and contain organic matter similar to Ivuna-type carbonaceous (CI) chondrites (*8*). We investigated two samples, both collected during the first Hayabusa2 touchdown operation on 2019 February 21 (*7, 9*).

Our main analysis was performed on an aggregate sample designated A0106 (fig. S1), consisting of grains less than 1 mm diameter with a total weight of 38.4 mg, which has elsewhere been investigated spectroscopically (*10*), and had its elemental and isotopic compositions analyzed (*11*). The A0106 sample has typical mineralogy for Ryugu, consisting mainly of hydrous silicate minerals, including serpentine and saponite, with other associated minerals such as dolomite, pyrrhotite and magnetite, indicating extensive aqueous alteration (*10*). We used solvent extracts to investigate the organic molecule content of A0106, following the analysis scheme in fig. S2. We also analyzed a single ~1 mm-sized grain (A0080) to determine the spatial distribution of organic compounds on its surface, using in-situ analysis methods (fig. S2).

Elemental and isotopic composition

Elemental and isotopic analyses were performed using mass spectrometry (*11*). The A0106 sample contains 3.76 ± 0.14 wt.% of total carbon (C), 1.14 ± 0.09 wt.% of total hydrogen (H), 0.16 ± 0.01 wt.% of total nitrogen (N), and 3.3 ± 0.7 wt.% of total sulfur (S). The concentration of pyrolyzed oxygen (O), liberated at 1400ºC under a helium gas flow, was 12.9 ± 0.42 wt.%. The total CHNOS content (~21.3 wt.%) is likely to comprise hydrous minerals, carbonates, sulfides and organics, including macromolecular insoluble organic matter and SOM, because these are detected in other Ryugu samples (*10, 12*). The stable isotopic compositions were determined and are expressed in δ notations as offsets from international standards (*11*): $\delta^{13}C = -0.58 \pm 2.0$ ‰ relative to Vienna Peedee Belemnite (VPDB), $\delta D = +252 \pm 13$ ‰ relative to Vienna Standard Mean Ocean Water (VSMOW), $\delta^{15}N = +43.0 \pm 9.0$ ‰ relative to Earth atmospheric nitrogen, $\delta^{34}S = -3.0 \pm 2.3$ ‰ relative to Vienna Canyon Diablo Troilite (VCDT), and $\delta^{18}O = +12.6 \pm 2.0$ ‰ relative to VSMOW [all analyses in triplicate (*11*)]. Because we analyzed small aggregate grains from the first touchdown site, we consider these values representative of the average bulk

composition of Ryugu. The corresponding elemental ratios (by weight) are: C/N ratio = 23.5 ± 0.4, O/H ratio = 11.4 ± 0.6, C/S ratio = 1.15 for A0106 (table S1).

The C, N and H abundances are at the top of the ranges previously measured for carbonaceous chondrites (Fig. 1A-D, table S2). Our measured abundances of C, H and S are consistent with an independent bulk chemical analysis using ~25 mg of the Ryugu samples, which concluded that Ryugu has a composition more similar to CI chondrites than to other types of meteorite (*12*). The heavy isotope enrichments of H (δD ~ +250 ‰) and N ($\delta^{15}N$ ~ +40 ‰) we find in Ryugu are similar to previous analyses of the Ivuna and Orgueil CI chondrites (*13*) (Fig. 1E, F). However, elemental and isotopic heterogeneities on small scales have been found in other Ryugu samples (*14, 15*).

Diversity of organic molecules

We performed mass spectrometry on a methanol extract of the A0106 sample using electrospray ionization (ESI) and atmospheric pressure photoionization (APPI), coupled with Fourier transform-ion cyclotron resonance mass spectrometry (FT-ICR/MS) (*11*). These produced hundreds of thousands of ion signals with a mass to charge ratio (*m*/*z*) between 150 and 700 (Fig. 2A, B, F). The *m*/*z* signals obtained by negative charge ESI [ESI(-)], positive charge ESI [ESI(+)] and positive charge APPI [APPI(+)] were assigned to almost 20,000 elementary compositions, consisting of C, H, N, O and/or S (Fig. 2C-F, fig. S3). This diversity of compounds is consistent with previous results for carbonaceous chondrites (*16*). The chemical diversity of ionizable species (small molecules detectable with mass spectrometry) is much higher than terrestrial biological samples.

We identify a continuum of small molecules to macromolecules, with a range of carbon oxidation states from nonpolar or minimally polar (CH-containing, polycyclic aromatic hydrocarbons and branched aliphatic molecules) to polar small molecules (CHO-containing) with various functional groups (CHN, CHS, CHNO, CHOS, or CHNOS), having different solubility. The most intense signals in the mass spectra were assigned to polythionates (Fig. 2A), indicating formation through a complex sulfur polymer chemistry, governed by redox processes involving water-mineral interactions with metal sulfides. A homologous series of known molecular targets (CHN^+, $CHNO^+$) has previously been observed in a solvent extract of the Murchison meteorite, a different type of carbonaceous chondrite (*17*). The Ryugu data contain abundant series of signals with repetitive mass differences, which we interpret as evidence for a systematic reaction network including methylation, hydration, hydroxylation and sulfurization. We did not detect magnesium-containing organic compounds (such as CHOMg or CHOSMg), which have been observed in other chondritic meteorites including Murchison (*18*). The compound distribution indicates low temperature ($\lesssim$ 150 ºC) hydrothermal processing on Ryugu's parent body (*19*). The high diversity of N- and S-bearing molecules in Ryugu indicates chemical processes occurred involving nitrogen and sulfur chemistry (*20, 21*).

Amino acids

We searched for amino acids in an acid-hydrolyzed, hot water extract of the A0106 sample using a combination of 3-dimensional high performance liquid chromatography with a high-sensitivity fluorescence detector (3D-HPLC/FD) at Kyushu University, and ultrahigh performance liquid chromatography with fluorescence detection and high-resolution mass spectrometry (LC-FD/HRMS) at Goddard Space Flight Center (Fig. 3 and table S3). A total of 15 amino acids were

both detected and quantified, while an additional 5 amino acids were tentatively identified but not quantified. These included proteinogenic (used by biology to form proteins) amino acids such as glycine ($C_2H_5NO_2$), D,L-alanine ($C_3H_7NO_2$) and D,L-valine ($C_5H_{11}NO_2$), as well as the non-proteinogenic amino acids including β-alanine ($C_3H_7NO_2$), D,L-α-amino-*n*-butyric acid ($C_4H_9NO_2$), D,L-β-amino-*n*-butyric acid ($C_4H_9NO_2$), and several isomers of valine: D,L-norvaline, D,L-isovaline, and δ-amino-*n*-valeric acid (Fig. 3). The concentrations of each amino acid ranged from ~0.01 to 5.6 nmol g^{-1} (table S3).

Many of the non-proteinogenic amino acids identified in the Ryugu extract are rare or non-existent in terrestrial biology. The chiral amino acids detected in Ryugu are in approximately racemic mixtures [the abundance of the D- and L-enantiomers are approximately equal (D/L ~ 1)], indicating non-biological origins. The detection of approximately equal amounts of D- and L-alanine, a common proteinogenic amino acid, indicates that this Ryugu sample is pristine, with negligible biological L-amino acid contamination. However, there were excesses of L-serine and L-valine. There was a trace (pico-mole levels) of L-valine content in procedural solvent blanks, so contamination is likely the cause of the non-racemic valine in the A0106 extract.

There are differences in the amino acid concentrations measured using LC-FD/HRMS and 3D-HPLC/FD, which we attribute to different acid hydrolysis conditions and analytical techniques. Different sample preparation and analysis approaches are known to yield distinct results when investigating meteorite amino acids (*22*). The much lower glycine abundances measured by LC-FD/HRMS (~0.6 nmol g^{-1}) than by 3D-HPLC/FD (5.6 nmol g^{-1}) could have been the result of multiple evaporation steps implemented during sample preparation prior to LC-FD/HRMS analysis. These evaporation steps could have resulted in the additional loss of volatile species, such as hydrogen cyanide (HCN) and formaldehyde. HCN, formaldehyde, and ammonia can synthesize glycine under alkaline conditions (Strecker synthesis) such as during sample preparation (*11*).

The overall amino acid distribution in the Ryugu extract is distinct from that in the CI meteorite Orgueil, with Ryugu also having lower amino acid abundances than Orgueil (*23*) (table S3). This could reflect different chemical formation environments, or subsequent alteration conditions on their parent bodies. It is possible that Strecker synthesis could have been active during parent body aqueous alteration, producing glycine and other α-amino acids (those with an amino group one bond away from a carbonyl carbon) identified in the Ryugu extract. However, other amino acid formation and fractionation mechanisms must also have occurred on the Ryugu parent body, because β-, γ-, and δ-amino acids were also found (table S3). The straight-chain *n*-ω-amino acids, β-alanine, γ-amino-*n*-butyric acid, and δ-amino-*n*-valeric acid have higher abundances than other amino acids measured by LC-FD/HRMS in the Ryugu extract (table S3). This trend was similarly observed in previous measurements of thermally altered CO (Omans-type) and CV (Vigarano-type) carbonaceous chondrites (*24*). These non-α-amino acids have been shown to be more resistant to thermal decomposition, surviving at temperatures up to ~300ºC (*25, 26*), which could explain their higher abundances (relative to α-amino acids) in the Ryugu sample.

Aliphatic amines and carboxylic acids

Hot water extracts of A0106 were measured using liquid chromatography with fluorescence detection and time-of-flight mass spectrometry (LC-FD/ToFMS) (*11*). Aliphatic amines were detected (Fig. 4); methylamine (CH_3NH_2) was the most abundant followed by ethylamine ($C_2H_5NH_2$) and isopropylamine ($(CH_3)_2CHNH_2$), then *n*-propylamine ($C_3H_7NH_2$). These amines are likely present as salts in the grains, because the free amines are highly volatile and reactive

(boiling point; −6.3ºC for free CH_3NH_2 at 1013 hPa, compared to ~230ºC for CH_3NH_2 hydrochloride at ~0.11 Pa). We applied the same technique to hexane and dichloromethane (DCM) extracts of A0106, but did not find other volatile compounds that have previously been detected in carbonaceous chondrites, such as methanol (CH_3OH), ethanol (C_2H_5OH), methyl formate ($HCOOCH_3$), acetone (CH_3COCH_3), diethyl ether ($C_2H_5OC_2H_5$), or acetonitrile (CH_3CN), which were all below the detection limits (fig. S4). This is consistent with our interpretation that the amines were retained as salts, not trapped volatiles in inclusions, insoluble organic material or minerals. Ammonium salts (and amine salts) are known to be the major reservoir of nitrogen on the dwarf planet Ceres and in comets (*27, 28*). A previous hyperspectral microscope study of Ryugu grains found evidence of amine or ammonium bonds (NH; ~3.1 μm) (*29*).

Isopropyl amine, which has a branched chain, was more abundant than straight-chain propylamine. This is consistent with previous results for several carbonaceous chondrites (*30, 31*). The predominance of branched chains could indicate synthesis of these molecules occurred by a radical reaction. Alternatively, it might indicate a period of heating during aqueous alteration, because branched-chain carbon compounds are more thermodynamically stable than their straight-chain counterparts. The presence of methyl-, ethyl-, and propylamines in Ryugu is distinct from Orgueil, which contains butylamines ($C_4H_9NH_2$) at about half the abundance of *n*-propylamine (*32*); if this same ratio occurred in the Ryugu sample, butylamines would have been above the detection limits. The amines in Ryugu are also unlike the dust grains collected from the comet Wild 2 by the Stardust mission, for which only methyl- and ethylamine were detected (*33*).

Monocarboxylic acids (MCAs) were searched for using gas chromatography quadrupole mass spectrometry (GC-QMS) of the hot water extract of A0106. Formic acid (5.7 μmol g^{-1}) and acetic acid (9.5 μmol g^{-1}) were detected, the only MCAs above the detection limits (fig. S5, table S4). MCAs are typically among the most abundant organic compounds in organic rich carbonaceous chondrites, such as the CM (Mighei-type) meteorites Murchison and Murray, and the CR (Renazzo-type) chondrites (*34-36*). We detected MCAs in A0106 with high concentrations and low molecular diversity, both consistent with low-temperature hydrothermal processing, as thought to have occurred on Ryugu's parent body (*10*). The concentration of MCAs is known to decrease with increasing aqueous and/or thermal alteration experienced by meteorite samples (*36-37*). Although MCAs in A0106 have low molecular diversity, the concentrations of formic and acetic acids are high, similar to those observed in highly aqueously altered carbonaceous chondrites including ALH 83100 (a CM), Orgueil and Ivuna (both CIs) (*38, 39*). Aliphatic MCAs are substantially more abundant in the Ryugu sample than other structurally related organics, such as aliphatic amino acids and amines. This is consistent with carbonaceous chondrites, for which the concentrations of MCAs (and most other meteoritic organic compounds) are known to decrease with increasing molecular weight (*1, 36*). We find the same relationship between formic acid and acetic acid in A0106 (table S4).

Polycyclic aromatic hydrocarbons

We applied two-dimensional gas chromatography with time-of-flight mass spectrometry (GC×GC-TOFMS) to the organic solvent extracts of the A0106 sample. We detected aromatic hydrocarbons at below parts per million (sub-ppm) abundances, including from alkylbenzenes and polycyclic aromatic hydrocarbons (PAHs) (Fig. 5). Homologous series of large alkylated PAHs were identified using APPI FT-ICR/MS, and assigned to methylation and hydration (Fig. 2C). The presence of alkylated PAHs (including alkylbenzenes) in the organic solvent extracts was confirmed using Fourier-transformed infrared (FTIR) spectroscopy (*11*), which showed bands due

to CH_2 or CH_3 bonds at 2850 to 2950 cm^{-1} (3.51 to 3.39 μm) (fig. S6A). The highest abundance PAHs were fluoranthene and pyrene (which contain four benzene rings) followed by chrysene/triphenylene (also four rings) and methylated fluoranthene and pyrene. Smaller PAHs containing two rings (naphthalene) and three rings (phenanthrene and anthracene) were detected at lower abundances.

Fluoranthene and pyrene are structural isomers (both have the formula $C_{16}H_{10}$) that are present in roughly equal amounts in CM chondrites (*40-42*). In the Ryugu sample, however, fluoranthene is substantially less abundant than pyrene (Fig. 5C). In the CI meteorite Ivuna, both fluoranthene and pyrene are below the detection limits, though phenanthrene and anthracene are abundant (*43*). Because selective synthesis is not expected to favor three- or four-ring PAHs, their variable relative abundances in meteorites could be due to aqueous fluid flow in their parent body. It has been proposed that three-ring and four-ring PAHs could be spatially separated during aqueous alteration of the Ivuna parent body, due to their different aqueous solubilities (an effect known as asteroidal chromatography) (*44*). On Earth, hydrothermal petroleum often contains alkylbenzene and lower abundances of fluoranthene than of pyrene (*45*). Therefore, the difference in proportions of PAHs between Ryugu and carbonaceous chondrites could be due to different aqueous alteration effects on different parent bodies. However, we cannot rule out the possibility that the different proportions could be inherited from pre-solar syntheses in the interstellar medium, where PAHs are ubiquitous (*46*). PAHs with higher stability and lower volatility might have preferentially survived accretionary and hydrothermal processes on the parent body. For example, the higher thermal stability and lower volatility of pyrene over fluoranthene could have contributed to the unequal abundances of the two species in the Ryugu sample. Vaporization fractionation could be responsible for the lower abundance (compared to pyrene) of smaller PAHs, such as naphthalene.

The FTIR spectrum of the fine suspended material in the water extract of the A0106 grain (fig. S6C) has its strongest absorption band at ~1000 cm^{-1} (~10 μm) due to silicates (Si-O bonds). Other bands are present at 750 to 1650 cm^{-1} (13.3 to 6.1 μm). Peaks at these wavelengths have often been observed in the interstellar medium (*47*) and have been assigned to large PAHs (*47-50*). The broad peaks at ~1400 cm^{-1} (7.14 μm) could also have a contribution from carbonates (*51*). The lack of the aromatic C-H stretching bands at ~3030 cm^{-1} (3.30 μm) suggests that the PAHs present in the Ryugu water extract are highly depleted in hydrogen, indicating large unsaturated structures. Because small to moderate-size PAHs can be extracted with organic solvents such as DCM and methanol (MeOH), which we applied before extraction with water (fig. S2), we expect the PAHs suspended in the water extract to be dominated by very large and less soluble molecules that were not removed by the earlier analysis steps. The FTIR spectrum of the Ryugu sample is unlike those of other extraterrestrial materials, including carbonaceous chondrites. It is most similar to astronomical observations of interstellar PAHs (*50*), so it is possible that pre-solar PAHs (formed in the interstellar medium) were incorporated into Ryugu's parent body during its accretion, then survived the subsequent aqueous alteration.

N-containing heterocyclic compounds

The methanol extract of A0106 was examined using nano-liquid chromatography/high-resolution mass spectrometry (nanoLC/HRMS) (*11*). Several classes of alkylated N-containing heterocyclic molecules were identified, and their presence was confirmed using ESI FT-ICR/MS (Fig. 2E). These alkylated N-heterocycles included pyridine, piperidine, pyrimidine, imidazole or pyrrole rings with various amounts of alkylation (Fig. 6A). Alkylpyridines and alkylimidazoles (aromatic N-heterocycles) have previously been found in CM chondrites, while alkylpiperidines

(aliphatic N-heterocycles) are more abundant in CR chondrites (*52*); the difference in relative abundances might reflect differing redox conditions on the meteorite parent bodies.

The alkylpyridine ($C_nH_{2n-4}N^+$) homologues we identify in the Ryugu sample (Fig. 6B) have a different distribution pattern from those in CM chondrites (Fig. 6C). The number of carbon atoms in the Ryugu compounds is mostly between 11 and 22, with a maximum at 17, while the carbon number distribution for Murchison has a lower range, mostly from 8 to 16 with its maximum at 11. This difference could be caused by differences in the histories of hydrothermal activity (such as the water/rock ratio), solar radiation and/or cosmic ray irradiation (*53, 54*). Gas phase reactions at high temperature can produce polymeric series of N-containing heterocyclic compounds, like those found in meteorites (*55*). If the bell-shaped distributions for Ryugu and Murchison are due to gas-phase synthesis, the two bodies could have inherited their SOM from different regions of the solar nebula.

Alternatively, N-heterocyclic compounds can be synthesized through a reaction pathway using ammonia and simple aldehydes, such as formaldehyde (*56*), which would require high abundances of aldehyde and ammonia in the Ryugu body in the past. Because formaldehyde and ammonia were abundant in the interstellar medium and the proto-solar nebula (*57, 58*), the Ryugu organic material might have inherited these characteristics from a molecular cloud environment. In interstellar-ice analog experiments at very low temperature, hexamethylenetetramine (HMT: $C_6H_{12}N_4$) is produced as a major compound from single carbon compounds and ammonia (*59*). However, we did not detect HMT in any extracted fraction of our sample, using FT-ICR/MS and nanoLC/HRMS. HMT has previously been detected in aqueous extracts of carbonaceous meteorites including Murchison (*60*). Under hydrothermal conditions, HMT is degraded to formaldehyde and ammonia at ~150ºC, especially at alkaline pH, producing N-containing compounds such as amino acids and N-heterocycles (*61, 62*). Because the aqueous fluid on Ryugu's parent body was probably alkaline (pH > 9) (*10*), we attribute the lack of HMT to the aqueous alteration history.

Sample surface distribution of organic molecules

We performed in situ analysis of the surface of the A0080 grain using electrically-charged MeOH spraying by desorption electrospray ionization (DESI) coupled with HRMS (*11*). We detected over 200 positive ion peaks, ranging from m/z = 80 to 400, which we assign to molecules containing the elements CHN, CHO or CHNO and their alkylated homologues (Fig. 7, fig. S7). These compounds were located on the uppermost layer of the intact grain surface; no treatment (such as cutting or polishing) was performed on A0080. Methanol spraying detached the molecules from the surface, implying weak interactions between the CHN compounds and the major minerals of the grain. The CHN compounds observed were mostly consistent with those detected in the methanol extract of the aggregate sample (A0106); however, the molecular distribution was not identical (Fig. 6A, fig. S7B,C). We attribute the different molecular distributions to heterogenous distribution of the SOM compounds between the Ryugu grains, and/or differences in sensitivity between the two analytical methods.

Our molecular imaging shows spatial heterogeneity of the compounds across the surface of A0080 (Fig. 7). We expect the ion intensity to depend on the topography of the sample surface, which was not flattened. Although the region with highest SOM concentration is also the highest topographical area, the molecular imaging shows μm-scale differences in spatial distribution of the CHN compounds, depending on their molecular sizes and families (Fig. 7). Varying spatial

distribution among different molecular sizes and compound classes were also observed among CHO and CHNO compounds. Previous studies have identified different spatial distributions of CHN compounds on CM chondrites including Murray (*63*). The distinct distributions could be due to interactions between organic molecules and minerals during aqueous alteration (*64*). Other synthesis routes could also explain these results, for example via SOM reactions with minerals and fluids in the Ryugu parent body (*65*).

Implications for asteroid organic chemistry

The molecular diversity of SOM in the Ryugu sample A0106 is as high as previously found for carbonaceous chondrites, and includes poly-sulfur-bearing species. In contrast, the molecular diversity of low-molecular-weight compounds, including aliphatic amines and carboxylic acids, was lower in the Ryugu sample than previously measured in the Murchison meteorite. The total SOM concentration in the A0106 sample was less than that of Murchison, closer to those of the unheated CI chondrites Ivuna and Orgueil.

The Ryugu organic matter seems to have been affected by aqueous alteration, which produced aromatic hydrocarbons similar to hydrothermal petroleum on Earth (*45*). However, the Ryugu samples have never experienced high temperatures (*12*). This is unlike the heated CI chondrites Yamato 980115 and Belgica 7904 (parent body temperatures $\lesssim$150°C (*66, 67*)), which contain very low (or undetectable) abundances of amino acids and PAHs (*23, 68, 69*). Remote-sensing observations of Ryugu, collected by the Hayabusa2 spacecraft, showed evidence for thermal metamorphism at 300-400ºC on Ryugu's parent body (*70*). However, we estimate the effective heating temperature was $\lesssim$150ºC for the Ryugu SOM (*11*). We ascribe this difference to protection of the organics, by incorporation into hydrous minerals.

The SOM detected in the A0106 and A0080 samples indicates that Ryugu's surface materials host organic molecules, despite the harsh environment caused by solar heating, ultraviolet irradiation, cosmic-ray irradiation and high vacuum. The uppermost surface grains on Ryugu protect organic molecules - unlike meteorites, for which atmospheric ablation during Earth entry removes or modifies analogous near-surface material. Organic compounds on asteroids can be ejected from the surface by impacts or other causes (*71, 72*), dispersing them through the Solar System (or beyond) as meteoroids or interplanetary dust particles. Therefore, SOM on C-type asteroids could be a source of organics delivered to other bodies.

References and Notes

1. D. P. Glavin et al., The origin and evolution of organic matter in carbonaceous chondrites and links to their parent bodies. in *Primitive Meteorites and Asteroids*, N. Abreu, Ed. (Elsevier, 2018), pp. 205-271. doi: 10.1016/B978-0-12-813325-5.00003-3
2. E. Anders, Pre-biotic organic matter from comets and asteroids. *Nature* **342**, 255-257 (1989). doi: 10.1038/342255a0
3. C. Chyba, C. Sagan, Endogenous production, exogenous delivery and impact-shock synthesis of organic molecules: an inventory for the origins of life. *Nature* **355**, 125-132 (1992). doi: 10.1038/355125a0
4. F. E. DeMeo, B. Carry, Solar System evolution from compositional mapping of the asteroid belt. *Nature* **505**, 629-634 (2014). doi: 10.1038/nature12908

5. T. Hiroi, C. M. Pieters, M. E. Zolensky, M. E. Lipschutz, Evidence of thermal metamorphism on the C, G, B, and F asteroids. *Science* **261,** 1016–1018 (1993). doi: 10.1126/science.261.5124.1016

6. K. Kitazato et al., The surface composition of asteroid 162173 Ryugu from Hayabusa2 near-infrared spectroscopy. *Science* **364,** 272–275 (2019). doi: 10.1126/science.aav7432

7. S. Tachibana et al., Pebbles and sand on asteroid (162173) Ryugu: In situ observation and returned particles from two landing sites. *Science*, **375,** 1011-1016 (2022). doi: 10.1126/science.abj8624

8. T. Yada et al., Preliminary analysis of the Hayabusa2 samples returned from C-type asteroid Ryugu. *Nature Astron.*, **6,** 214-220 (2022). doi: 10.1038/s41550-021-01550-6

9. T. Morota et al., Sample collection from asteroid (162173) Ryugu by Hayabusa2: Implications for surface evolution. *Science* **368,** 654–659 (2020). doi: 10.1126/science.aaz6306

10. T. Nakamura et al., Formation and evolution of carbonaceous asteroid Ryugu: Direct evidence from returned samples. *Science*, eabn8671 (2022). doi: 10.1126/science.abn8671

11. Materials and methods are available as supplementary materials.

12. T. Yokoyama et al., Samples returned from the asteroid Ryugu are similar to Ivuna-type carbonaceous meteorites. *Science*, eabn7850 (2022). doi: 10.1126/science.abn7850

13. J. F. Kerridge, Carbon, hydrogen and nitrogen in carbonaceous chondrites: Abundances and isotopic compositions in bulk samples. *Geochim. Cosmochim. Acta* **49**, 1707-1714 (1985). doi: 10.1016/0016-7037(85)90141-3

14. R. Okazaki et al., Noble gases and nitrogen in samples of asteroid Ryugu record its volatile sources and recent surface evolution. *Science*, eabo0431 (2022). doi: 10.1126/science. abo0431

15. H. Yabuta et al., *Science*, this issue

16. P. Schmitt-Kopplin, Z. Gabelica, R. D. Gougeon, A. Fekete, B. Kanawati, M. Harir, I. Gebefuegi, G. Eckel, N. Hertkorn, High molecular diversity of extraterrestrial organic matter in Murchison meteorite revealed 40 years after its fall. *Proc. Natl Acad. Sci. U.S.A.*, **107**, 2763-2768 (2010). doi: 10.1073/pnas.0912157107

17. J. Hertzog, H. Naraoka, P. Schmitt-Kopplin, Profiling Murchison soluble organic matter for new organic compounds with APPI- and ESI-FT-ICR MS, *Life*, **9**, 48 (2019). doi: 10.3390/life9020048

18. A. Ruf, B. Kanawati, N. Hertkorn, Q.-Z. Yin, F. Moritz, M. Harir, M. Lucio, B. Michalke, J. Wimpenny, S. Shilobreeva, B. Bronsky, V. Saraykin, Z. Gabelica, R. D. Gougeon, E. Quirico, S. Ralew, T. Jakubowski, H. Haack, M. Gonsior, P. Jenniskens, N.W. Hinman, P. Schmitt-Kopplin, Previously unknown class of metalorganic compounds revealed in meteorites. *Proc. Natl Acad. Sci. U.S.A.*, **114**, 2819-2824 (2017). doi: 10.1073/pnas.1616019114

19. M. Matzka, M. Lucio, B. Kanawati, E. Quirico, L. Bonal, S. Loehle, P. Schmitt-Kopplin, Thermal history of asteroid parent bodies is reflected in their metalorganic chemistry. *Astrophys. J. Lett.* **915**, L7 (2021). doi: 0.3847/2041-8213/ac0727

20. G. Danger, V. Vinogradoff, M. Matzka, L. Remusat, S. Bernard, A. Ruf, L. Le Sergeant d'Hendecourt, P. Schmitt-Kopplin, From molecular clouds to chondrites: Exploring the link between molecular cloud ices and chondritic organics, *Nature commun.*,**12**, 3538 (2021). doi: 10.1038/s41467-021-23895-2

21. A. Ruf, A. Bouquet, P. Schmitt-Kopplin, O. Boduch, O. Mousis, G. Danger, Sulfur ion irradiation experiments simulating space weathering of Solar System body surfaces compound formation, *Astronom. Astrophys.*, **655**, A74 (2021). doi: 10.1051/0004-6361/202141190

22. D. N. Simkus, J. C. Aponte, J. E. Elsila, E. T. Parker, D. P. Glavin, J. P. Dworkin, Methodologies for analyzing soluble organic compounds in extraterrestrial samples: Amino acids, amines, monocarboxylic acids, aldehydes, and ketones. *Life* **9**, 47 (2019). doi: 10.3390/life9020047

23. A. Burton, S. Grunsfeld, J. Elsila, D. Glavin, J. Dworkin, The effects of parent-body hydrothermal heating on amino acid abundances in CI-like chondrites. *Polar Science* **8**, 255 - 263 (2014). doi: 10.1016/j.polar.2014.05.002

24. A. Burton, J. Elsila, M. P. Callahan, M. G. Martin, D. P. Glavin, N. M. Johnson, J. Dworkin, A propensity for *n*-ω-amino acids in thermally altered Antarctic meteorites. *Meteorit. Planet. Sci.* **47**, 374-386 (2012). doi: 10.1111/j.1945-5100.2012.01341.x

25. Md. N. Islam, T. Kaneko, K. Kobayashi, Reaction of amino acids in a supercritical water-flow reactor simulating submarine hydrothermal systems. *Bull. Che. Soc. Jpn* **76**, 1171-1178 (2003). doi: 10.1246/bcsj.76.1171

26. J. Li, T. B. Brill, Spectroscopy of hydrothermal reactions, part 26: kinetics of decarboxylation of aliphatic amino acids and comparison with the rates of racemization. *Int. J. Chem. Kinetics* **35**, 602-610 (2003). doi: 10.1002/kin.10160

27. M. C. De Sanctis, E. Ammannito, A. Raponi, et al., Ammoniated phyllosilicates with a likely outer Solar System origin on (1) Ceres. *Nature* **528**, 241-244 (2015). doi.org/10.1038/nature16172

28. O. Poch et al., Ammonium salts are a reservoir of nitrogen on a cometary nucleus and possibly on some asteroids. *Science* **367**, eaaw7462 (2020). doi: 10.1126/science.aaw7462

29. C. Piloget et al., First compositional analysis of Ryugu samples by MicrOmega hyperspectral microscope. *Nature Astron.* **6,** 221-225 (2022). doi: 10.1038/s41550-021-01549-z

30. J. C. Aponte, J. P. Dworkin, J. E. Elsila, Assessing the origins of aliphatic amines in the Murchison meteorite from their compound-specific carbon isotopic ratios and enantiomeric composition. *Geochim. Cosmochim. Acta* **141**, 331-345 (2014). doi: 10.1016/j.gca.2014.06.035

31. J. C. Aponte, H. L. McLain, J. P. Dworkin, J. E. Elsila, Aliphatic amines in Antarctic CR2, CM2, and CM1/2 carbonaceous chondrites. *Geochim. Cosmochim. Acta* **189**, 296-311 (2015). doi: 10.1016/j.gca.2016.06.018

32. J. C. Aponte, J. P. Dworkin, J. E. Elsila, Indigenous aliphatic amines in the aqueously altered Orgueil meteorite. *Meteorit. Planet. Sci.* **50**, 1733-1749 (2015). doi: 10.1111/maps.12507

33. D. P. Glavin, J. P. Dworkin, S. A. Sandford, Detection of cometary amines in samples returned by Stardust. *Meteorit. Planet. Sci.* **43**, 399-413 (2008). doi: 10.1111/j.1945-5100.2008.tb00629.x

34. G. U. Yuen, K. A. Kvenvolden, Monocarboxylic acids in Murray and Murchison carbonaceous meteorites. *Nature* **246**, 301-303 (1973). doi: 10.1038/246301a0

35. Y. Huang, et al., Molecular and compound-specific isotopic characterization of monocarboxylic acids in carbonaceous meteorite. *Geochim. Cosmochim. Acta* **69**, 1073-1084 (2005). doi: 10.1016/j.gca.2004.07.030

36. J. C. Aponte, H. K. Woodward, N. M. Abreu, J. E. Elsila, J. P. Dworkin, Molecular distribution, ^{13}C-isotope, and enantiomeric compositions of carbonaceous chondrite monocarboxylic acids. *Meteorit. Planet. Sci.* **54**, 415–430 (2019). doi: 0.1111/maps.13216

37. H. Naraoka, A. Shimoyama, K. Harada, Molecular distribution of monocarboxylic acids in Asuka carbonaceous chondrites from Antarctica. *Origins Life Evol. Biosph.* **29**, 187–201 (1999). doi: 10.1023/A:1006547127028

38. J. C. Aponte, M. R. Alexandre, Y. A. J. Brearley, C. M. O.'D. Alexander, Y. Huang, Effects of secondary alteration on the composition of free and IOM-derived monocarboxylic acids in carbonaceous chondrites. *Geochim. Cosmochim. Acta* **75**, 2309-2323 (2011). doi: 10.1016/j.gca.2011.01.040

39. J. C. Aponte, D. Whitaker, M. W. Powner, J. E. Elsila, J. P. Dworkin, Analyses of aliphatic aldehydes and ketones in carbonaceous chondrites. *ACS Earth Space Chem.* **3**, 463-472 (2019). doi: 10.1021/acsearthspacechem.9b00006

40. B. P. Basile, B. S. Middleditch, J. Oró, Polycyclic aromatic hydrocarbons in the Murchison meteorite. *Org. Geochem.* **5**, 211-216 (1984). doi: 10.1016/0146-6380(84)90008-1

41. H. Naraoka, A. Shimoyama, M. Komiya, H. Yamamoto and K. Harada, Hydrocarbons in the Yamato-791198 carbonaceous chondrite from Antarctica. *Chem. Lett.*, **17**, 831-834 (1988). doi: 10.1246/cl.1988.831

42. H. Naraoka, A. Shimoyama, K. Harada, Isotopic evidence from an Antarctic carbonaceous chondrite for two reaction pathways of extraterrestrial PAH formation. *Earth Planet. Sci. Lett.* **184**, 1-7 (2000). doi: 10.1016/S0012-821X(00)00316-2

43. M. R. Wing, J. L. Bada, The origin of the polycyclic aromatic hydrocarbons in meteorites. *Origins Life Evol. Biosph.* **21**, 375-383 (1992). doi: 10.1007/BF01808308

44. M. R. Wing, J. L. Bada, Geochromatography on the parent body of the carbonaceous chondrite Ivuna. *Geochim. Cosmochim. Acta* **55**, 2937-2942 (1991). doi: 10.1016/0016-7037(90)90458-H

45. B. R. T. Simoneit, P. F. Lonsdale, Hydrothermal petroleum in mineralized mounds at the seabed of Guaymas Basin. *Nature* **295**, 198-202 (1982). doi: 10.1038/295198a0

46. A. Leger, J. L. Puget, Identification of the "unidentified IR emission features of interstellar dust? *Astron. Astrophys.* **137**, L5-L8 (1984). bibcode: 1984A&A...137L...5L

47. E. Peeters, S. Hony, C. Van Kerckhoven, A. G. G. M. Tielens, L. J. Allamandola, D. M. Hudgins, C. W. Bauschlicher, The rich 6 to 9 μm spectrum of interstellar PAHs. *Astron. Astrophys.* **390**, 1089-1113 (2002). doi: 10.1015/0004-6361:20020773

48. S.R. Langhoff, Theoretical infrared spectra for polycyclic aromatic hydrocarbon neutrals, cations, and anions. *J. Phys. Chem. A*, **100**, 2819-2841 (1996). doi: 10.1021/jp952074g

49. B. T. Draine, A. Li, Infrared emission from interstellar dust. IV. The silicate-graphite model in the post-*SPITZER* era. *Astrophys. J.* **657**, 810–837 (2007). doi: 10.1086/511055

50. A. G. G. M. Tielens, Interstellar polycyclic aromatic hydrocarbon molecules. *Annu. Rev. Astron. Astrophys.* **46**, 289–337 (2008). doi: 10.1146/annurev.astro.46.060407.145211

51. G. Matrajt, J. Borg, P. I. Raynal, Z. Djouadi, L. d'Hendecourt, G. Flynn, D. Deboffle, FTIR and Raman analyses of the Tagish Lake meteorite: Relationship with the aliphatic hydrocarbons observed in the Diffuse Interstellar Medium. *Astron. Astrophys.* **416**, 983–990 (2004). doi: 10.1015/0004-6361:20034526

52. H. Naraoka, M. Hashiguchi, Distinct distribution of soluble N-heterocyclic compounds between CM and CR chondrites. *Geochem. J.* **53**, 33–40 (2019). doi: 10.2343/geochemj.2.0546

53. F.-R. Orthous-Daunay, L. Piani, L. Flandinet, et al. Ultraviolet-photon fingerprints on chondritic large organic molecules. *Geochem. J.* **53**, 21–32 (2019). doi: 10.2343/geochemj.2.0544

54. J. Isa, F.-R. Orthous-Daunay, P. Beck, C. D. K. Herd, V. Vuitton, L. Flandinet, Aqueous alteration on asteroids simplifies soluble organic matter mixtures. *Astrophys. J. Lett.* **920**, L39 (2021). doi: 10.3847/2041-8213/ac2b34

55. D. V. Bekaert, S. Derenne, L. Tissandier, Y. Marrocchi, S. Charnoz, C. Anquetil, B. Marty. High-temperature ionization-induced synthesis of biologically relevant molecules in the protosolar nebula. *Astrophys. J.* **859**, 142 (2018). doi: 10.3847/1538-4357/aabe7a

56. H. Naraoka, Y. Yamashita, M. Yamaguchi, and F-R. Orthous-Daunay. Molecular evolution of N-containing cyclic compounds in the parent body of the Murchison meteorite. *ACS Earth Space Chem.* **1**, 540–550 (2017). doi: 10.1021/acsearthspacechem.7b00058

57. P. Ehrenfreund, S. B. Charnley, Organic molecules in the interstellar medium, comets, and meteorites: a voyage from dark clouds to the early Earth. *Annu. Rev. Astron. Astrophys.* **38**, 427–483 (2000). doi: 10.1146/annurev.astro.38.1.427

58. J. Pegues, K. I. Öberg, J. B. Bergner, R. A. Loomis, C. Qi, R. Le Gal, L. I. Cleeves, V. V. Guzmán, J. Huang, J. K. Jørgensen, S. M. Andrews, G. A. Blake, J. M. Carpenter, K. R. Schwarz, J. P. Williams, D. J. Wilner, An ALMA Survey of H_2CO in Protoplanetary Disks. *Astrophys. J.* **890**,142 (2020). doi: 10.3847/1538-4357/ab64d9

59. M. P. Bernstein, S. A. Sandford, L. J. Allamandola, S. Chang, M. A. Scharberg, Organic compounds produced by photolysis of realistic interstellar and cometary ice analogs containing methanol. *Astrophys. J.* **454**, 327-344 (1995). doi: 10.1086/176485

60. Y. Oba, Y. Takano, H. Naraoka, Y. Furukawa, D. P. Glavin, J. P. Dworkin, S. Tachibana, Extraterrestrial hexamethylenetetramine in meteorites—a precursor of prebiotic chemistry in the inner solar system. *Nature Commun.* **11**, 6243 (2020). doi: 10.1038/s41467-020-20038-x

61. Y. Wolman, S. L. Miller, J. Ibanez, J, Oró, Formaldehyde and ammonia as precursors to prebiotic amino acids. *Science* **174**, 1039-1040 (1971). doi: 10.1126/science.174.4013.1038

62. V. Vinogradoff, S. Bernarda, C. Le Guilloub, L. Remusat, Evolution of interstellar organic compounds under asteroidal hydrothermal conditions. *Icarus* **305**, 358-370 (2018). doi: 10.1016/j.icarus.2017.12.019

63. H. Naraoka, M. Hashiguchi, In situ organic compound analysis on a meteorite surface by desorption electrospray ionization coupled with an Orbitrap mass spectrometer. *Rapid Commun. Mass Spectrom.* **32**, 959-964 (2018). doi: 10.1002/rcm.8121

64. K. Muneishi, H. Naraoka, Interactions between organic compounds and olivine under aqueous conditions: A potential role for organic distribution in carbonaceous chondrites. *Meteorit. Planet. Sci.* **56,** 195–205 (2021). doi: 10.1111/maps.13614

65. M. Hashiguchi, H. Naraoka, High-mass resolution molecular imaging of organic compounds on the surface of Murchison meteorite. *Meteorit. Planet. Sci.* 5**4**, 452–468. (2019). doi: 10.1111/maps.13211

66. R. N. Clayton, T. K. Mayeda, Oxygen isotope studies of carbonaceous chondrites. *Geochim. Cosmochim. Acta* **63**, 2089-2104 (1999). doi: 10.1016/S0016-7037(99)00090-3

67. A. J. King, H. C. Bates, D. Krietsch, H. Busemann, P. L. Clay, P. F. Schofield, S. S. Russell, The Yamato-type (CY) carbonaceous chondrite group: Analogues for the surface of asteroid Ryugu? *Geochemistry* **79**, 125531 (2019). doi: 10.1016/j.chemer.2019.08.003

68. A. Shimoyama, K. Harada, Amino acid depleted carbonaceous chondrites (C2) from Antarctica. *Geochem. J.* **18**, 281-286 (1984). doi: 10.2343/geochemj.18.281

69. Q. Chan, Y. Chikaraishi, Y. Takano, N. O. Ogawa, N. Ohkouchi, Amino acid compositions in heated carbonaceous chondrites and their compound-specific nitrogen isotopic ratios. *Earth, Planets Space* **68**, 7 (2016). doi: 10.1186/s40623-016-0382-8

70. E. Tatsumi et al., Spectrally blue hydrated parent body of asteroid (162173) Ryugu. *Nature Commun.* **12**, 5837 (2021). doi: 10.1038/s41467-021-26071-8

71. M. Arakawa et al., An artificial impact on the asteroid (162173) Ryugu formed a crater in the gravity-dominated regime. *Science* **368**, 67-71 (2020). doi: 10.1126/science.aaz1701

72. D. S. Lauretta et al. Episodes of particle ejection from the surface of the active asteroid (101955) Bennu. *Science* **366**, eaay3544 (2019). doi: 10.1126/science.aay3544

73. M. Ito et al., The universal sample holders of microanalytical instruments of FIB, TEM, NanoSIMS, and STXM-NEXAFS for the coordinated analysis of extraterrestrial materials. *Earth Planets Space* **72**, 133 (2020). doi: 10.1186/s40623-020-01267-2

74. H. Naraoka, https://data.darts.isas.jaxa.jp/pub/hayabusa2/paper/sample/Naraoka_2022/

75. N. O. Ogawa, T. Nagata, H. Kitazato, N. Ohkouchi, Ultra-sensitive elemental analyzer/isotope ratio mass spectrometer for stable nitrogen and carbon isotope analyses. *Earth, Life and Isotopes* (Edited by Ohkouchi N., Tayasu I. and Koba K.), Kyoto Univ Press, 339–353 (2010). ISBN: 4876989605

76. Y. Kebukawa et al., Primordial organic matter in the xenolithic clast in the Zag H chondrite: Possible relation to D/P asteroids. *Geochim. Cosmochim. Acta* **271**, 61–77 (2020). doi: 10.1016/j.gca.2019.12.012

77. Y. Kebukawa et al., Organic matter in carbonaceous chondrite lithologies of Almahata Sitta: Incorporation of previously unsampled carbonaceous chondrite lithologies into ureilitic regolith. *Meteorit. Planet. Sci.* **56**, 1311–1327 (2021). doi: 10.1111/maps.13713

78. B. E. Kornexl et al., On-line $\delta^{18}O$ measurements of organic and inorganic substances. *Rapid Commun. Mass Spectrom.* **13**, 1685-1693 (1999). doi: 10.1002/(SICI)1097-0231(19990830)13:16<1685::AID-RCM699>3.0.CO;2-9

79. G. Boato, The isotopic composition of hydrogen and carbon in the carbonaceous chondrites. *Geochim. Cosmochim. Acta* **6**, 209–220 (1954). doi: 10.1016/0016-7037(54)90001-0

80. F. Robert, L. Merlivat, M. Javoy, Deuterium concentration in the early Solar System: Hydrogen and oxygen isotope study. *Nature* **282**, 785–789 (1979). doi: 10.1038/282785a0

81. Y. Kolodny, J. Kerridge, I. Kaplan, Deuterium in carbonaceous chondrites. *Earth Planet. Sci. Lett.* **46**, 149–158 (1980). doi: 10.1016/0012-821X(80)90001-1

82. N. McNaughton, J. Borthwick, A. Fallick, C. Pillinger, Deuterium/hydrogen ratios in unequilibrated ordinary chondrites. *Nature* **294**, 639–641 (1981). doi: 10.1038/294639a0

83. F. Robert, S. Epstein, The concentration and isotopic composition of hydrogen, carbon and nitrogen in carbonaceous meteorites. *Geochim. Cosmochim. Acta* **46**, 81–95 (1982). doi: 10.1016/0016-7037(82)90293-9

84. J. Yang, S. Epstein, Interstellar organic matter in meteorites. *Geochim. Cosmochim. Acta* **47**, 2199–2216 (1983). doi: 10.1016/0016-7037(83)90043-1

85. F. Robert, The D/H ratio in chondrites. *Space Sci. Rev.* **106**, 87-101 (2003). doi: 10.1023/A:1024629402715

86. V. K. Pearson, M. Sephton, I. Gilmour, Molecular and isotopic indicators of alteration in CR chondrites. *Meteorit. Planet. Sci.* **41**, 1291–1303 (2006). doi: 10.1111/j.1945-5100.2006.tb00528.x

87. E. Jarosewich, Chemical analyses of meteorites at the Smithsonian Institution: An update. *Meteorit. Planet. Sci.* **41**, 1381–1382 (2006). doi: 10.1111/j.1945-5100.2006.tb00528.x

88. C. M. O'D. Alexander et al., The provenances of asteroids, and their contributions to the volatile inventories of the terrestrial planets. *Science* **337**, 721–723 (2012). doi: 10.1126/science.1223474

89. C. M. O'D. Alexander et al., A mutli-technique search for the most primitive CO chondrites. *Geochim. Cosmochim. Acta* **221**, 406–420 (2018). doi: 10.1016/j.gca.2017.04.021

90. L. G. Vacher et al., Hydrogen in chondrites: Influence of parent body alteration and atmospheric contamination on primordial components. *Geochim. Cosmochim. Acta* **281**, 53–66 (2020). doi: 10.1016/j.gca.2020.05.007

91. L. G. Vacher, Y. Marrocchi, M. J. Verdier-Paoletti, J. Villeneuve, M. Gounelle, Inward radial mixing of interstellar water ices in the solar protoplanetary disk. *Astrophys. J.* **827**, L1 (2016). doi: 10.3847/2041-8205/827/1/L1

92. L. Piani, H. Yurimoto, L. Remusat, A dual origin for water in carbonaceous asteroids revealed by CM chondrites. *Nature Astron.* **2**, 317–323 (2018). doi: 10.1038/s41550-018-0413-4

93. L. Piani et al., Earth's water may have been inherited from material similar to enstatite chondrite meteorites. *Science* **369**, 1110–1113 (2020). doi: 0.1126/science.aba1948

94. L. Piani, Y. Marrocchi, L. G. Vacher, H. Yurimoto, M. Bizzarro, Origin of hydrogen isotopic variations in chondritic water and organics. *Earth Planet. Sci. Lett.* **567**, 117008 (2021). doi: 10.1016/j.epsl.2021.117008

95. D. Tziotis, N. Hertkorn, P. Schmitt-Kopplin, Kendrick-analogous network visualisation of Ion Cyclotron Resonance Fourier Transform (FTICR) mass spectra: Improved options to assign elemental compositions and to classify organic molecular complexity. *Euro. J. Mass Spectrom.* **17**, 415–421 (2011). doi: 10.1255/ejms.1135

96. A. Furusho, T. Akita, M. Mita, H. Naraoka, K. Hamase, Three-dimensional high-performance liquid chromatographic analysis of chiral amino acids in carbonaceous chondrites. *J. Chromatogr. A* **1625**, 461255 (2020). doi: 10.1016/j.chroma.2020.461255

97. D. P. Glavin, et al., Amino acid analyses of Antarctic CM2 meteorites using liquid chromatography-time of flight-mass spectrometry. *Meteorit. Planet. Sci.* **41**, 889–902 (2006). doi: 10.1111/j.1945-5100.2006.tb00493.x

98. I. Boogers, W. Plugge, Y. Q. Stokkermans, A. L. Duchateau, Ultra-performance liquid chromatographic analysis of amino acids in protein hydrolysates using an automated pre-column derivatisation method. *J. Chromatog. A* **1189**, 406–409 (2008). doi: 10.1016/j.chroma.2007.11.052

99. J. C. Aponte, et al., Extraterrestrial organic compounds and cyanide in the CM2 carbonaceous chondrites Aguas Zarcas and Murchison. *Meteorit. Planet. Sci.* **55**, 1509–1524 (2020). doi: 10.1111/maps.13531

100. H. Naraoka, M. Hashiguchi, Y. Sato, K. Hamase, New applications of high-resolution analytical methods to study trace organic compounds in extraterrestrial materials. *Life* **9**, 62 (2019). doi: 10.3390/life9030062

101. BioMap, http://ms-imaging.org/biomap

Acknowledgments: The Hayabusa2 project has been led by JAXA (Japan Aerospace Exploration Agency) in collaboration with DLR (German Space Center) and CNES (French Space Center), and supported by NASA and ASA (Australian Space Agency). We thank all of the members of the Hayabusa2 project for their technical and scientific contributions.

Funding: Supported by the Japan Society for the Promotion of Science (JSPS) under KAKENHI grant numbers; JP20H00202 (H.N.), JP20H05846 (H.N.), JP20K20485 (S. Sak), JP20K14549 (H.S.), JP21J00504 (T.K.), JP21H01203 (N.O.O.), and JP21H04501 (Y.O), and JP21KK0062 (Y.T.). J.P.D., J.C.A., E.T.P., D.P.G., H.L.M., J.E.E., and H.V.G. are thank NASA for support under the Consortium for Hayabusa2 Analysis of Organic Solubles. F.-R.O.D. acknowledges support from CNES (grant BC_U53-6336-4500068838). J.M.E. is grateful for the NSF Graduate Research Fellowship “Emerging Worlds”, grant #18-EW18 2-0084.

Author contributions: H.N., Y.T., and J.P.D designed the research. Y.T., N.O.O., P.S.-K., K.H., A.F., J.C.A., E.T.P., D.P.G., H.L.M., Y.O., T.K., M.Has, K.F., D.A., F.-R.O.-D., C.W., J.I., S.Sak, T.Y., J.M.E., N.Her, J.P.D., and H.N. conducted experiments and analyzed data in cooperation with T.Yad, H.Yur, H.Yab, T.Nak, Y.C., N.Ohk, H.S., H.M., Y.F., A.R., V.V., R.T., H.C.C., and D.S.L.. H.N., Y.T., J.P.D., P.S.-K., H.V.G, J.E.E., K.H., A.F., Y.O., M.Has, F.-R.O.-D., J.I., and S.Tac. wrote the paper. M.Abe, T.Yad, M.N., K.Y., A.N., M.Y., A.S., A.Miy, S.F., K.Hat, H.Soe, Y.H., K.Kum, T.U., T.H., D.Y., and R.F. curated samples. K.Kit, S.Sug, N.N., M.Ara, H.I., M.I., Nar H., K.W., Y.I., R.N., T.Mor, N.S., K.M., H.S., R.H., E.T., Y.Y., C.H., T.Mic, M.M., A.Miu, H.Nod, T.Yam, K.Yos, K.Kaw, M.O., Y.I., H.Yan, M.Hay, T.I., R.T., H.Saw, S.H., K.O.,

C.O., Nao H., K.S., Y.S., M.Y., T.O., Y.Y., H.T., A.F., T.T., K.Y., Y.M., G.O., N.Oga, S.K., S.N., F.T., S.Tan, T.S., M.Y., S.W. and Y.T. contributed to the sample collection at Ryugu. All authors discussed the results and commented on the manuscript.

Competing interests: The authors declare no competing interests.

Data and materials availability: The mass spectra and chromatographic data used in this study are available at the JAXA Data Archives and Transmission System (DARTS) at https://data.darts.isas.jaxa.jp/pub/hayabusa2/paper/sample/Naraoka_2022/ *(73)*. Other data from the mission are available at the DARTS archive https://www.darts.isas.jaxa.jp/planet/project/hayabusa2/ and on the Small Bodies Node of the NASA Planetary Data System https://pds-smallbodies.astro.umd.edu/data_sb/missions/hayabusa2/. Material was allocated by the JAXA Astromaterials Science Research Group; the sample catalog is available at https://darts.isas.jaxa.jp/ curation/hayabusa2/, and distribution for analysis is through an Announcement of Opportunity available at https://jaxa-ryugu-sample-ao.net. The samples of Ryugu used in this study were mostly consumed during the analysis, with the remaining materials returned to JAXA.

Supplementary Materials

Materials and Methods

Supplementary Text

Figs. S1 to S8

Tables S1 to S5

References (*74–101*)

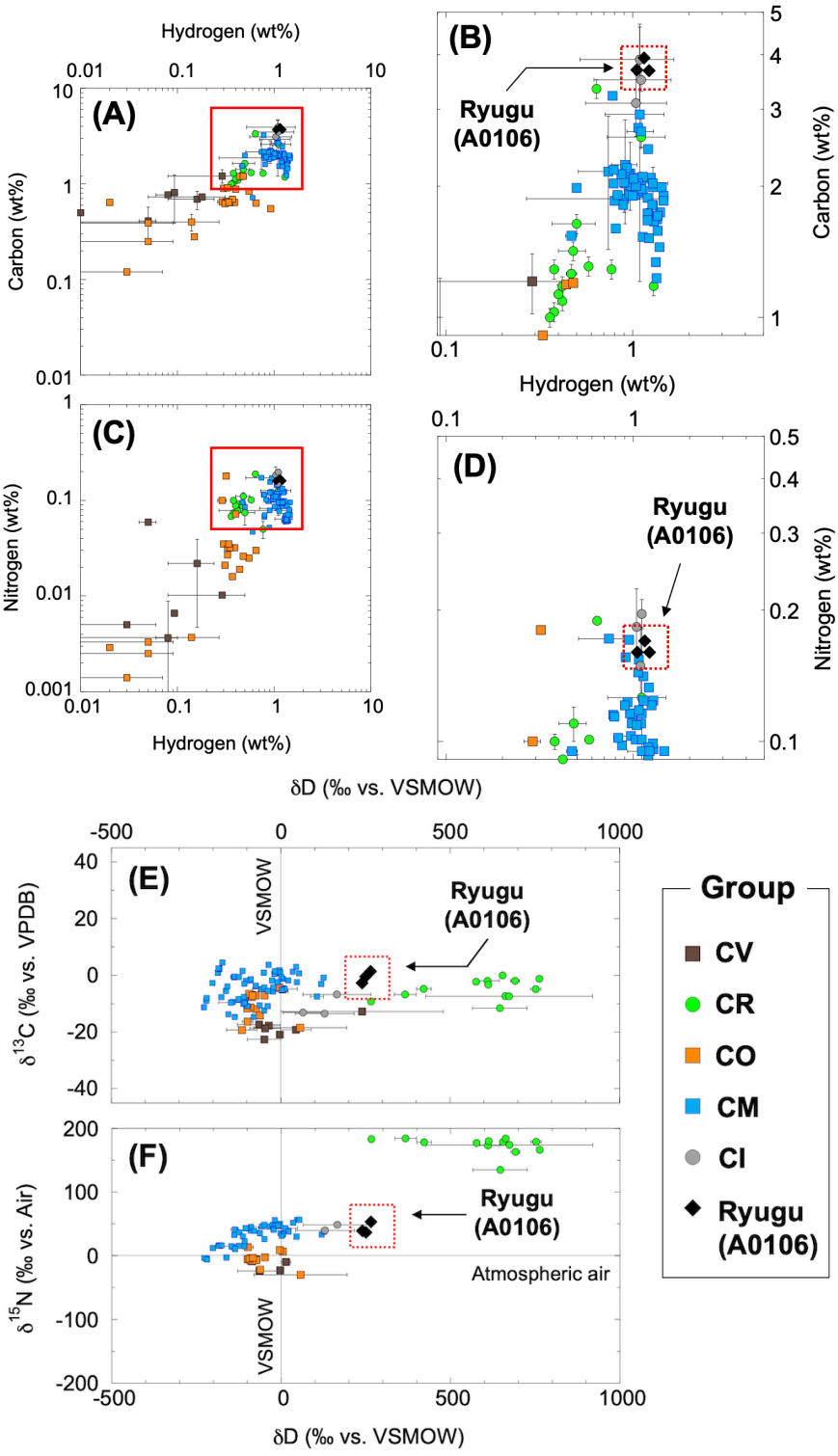

Fig. 1. Carbon, nitrogen, and hydrogen contents, and stable isotopic compositions, for the Ryugu sample A0106 compared with carbonaceous chondrites. (A) H-C (wt%), (B) enlarged H-C (wt%), (C) H-N (wt%), (D) enlarged H-N (wt%), (E) δD-δ^{13}C (‰), and (F) δD-δ^{15}N (‰). Symbols shown in the legend indicate different groups of carbonaceous chondrite: Vigarano-type (CV), Renazzo-type (CR), Ornans-type (CO), Mighei-type (CM) and Ivuna-type (CI). Ryugu is most similar to the CI chondrites. Data sources for the carbonaceous chondrites are listed in table

S2. Error bars are 1 standard deviation for C, H and δD, and 2 standard deviations for N, δ13C and δ15N.

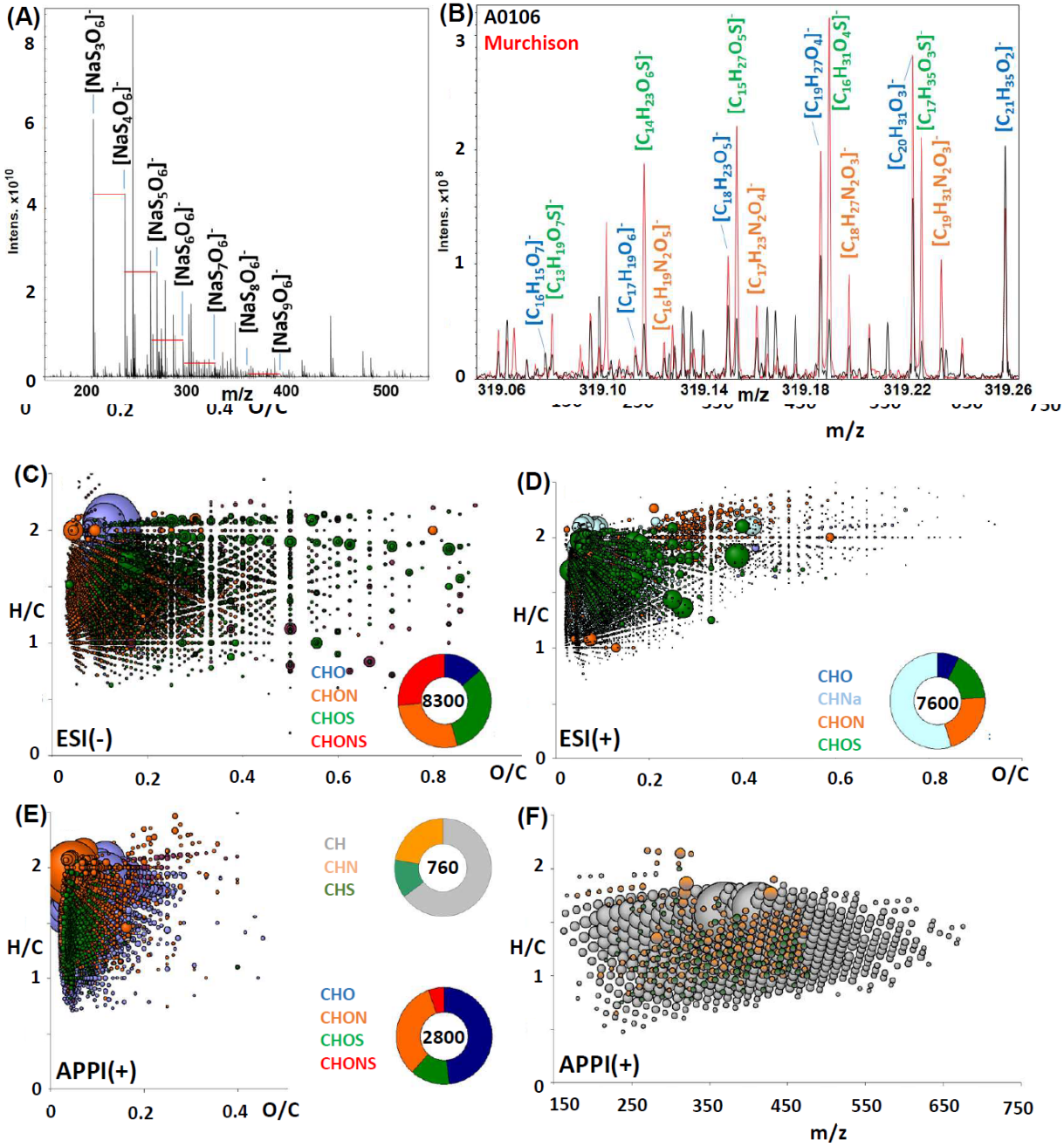

Fig. 2. Mass spectra of the Ryugu extract and derived elemental compositions. (A) Mass spectrum of negative ESI FTICR/MS with peaks assigned polythionates with 3 to 9 sulfur atoms. (B) Detail around *m*/*z* = 319 with annotated elementary compositions, with Ryugu (black) compared to the Murchison meteorite (red) (*16*); (C) O/C-H/C atomic ratios of the compositional data as obtained with ESI(-), (D) ESI(+), and (E) APPI(+). Colored annuli enclose the number of molecules assigned, with colors indicating the relative ratios of the chemical families (indicated in each legend). Data points use the same colors to indicate the family, and the size of each bubble indicates the intensity of the signal in the mass spectrum. (F) H/C atomic ratio as a function of *m*/*z*, measured using APPI(+), for non-oxygenated CH, CHN and CHS compositions; colors are the same as used in panel E. Figure S3 shows separate plots of each chemical family identified in panels C to E.

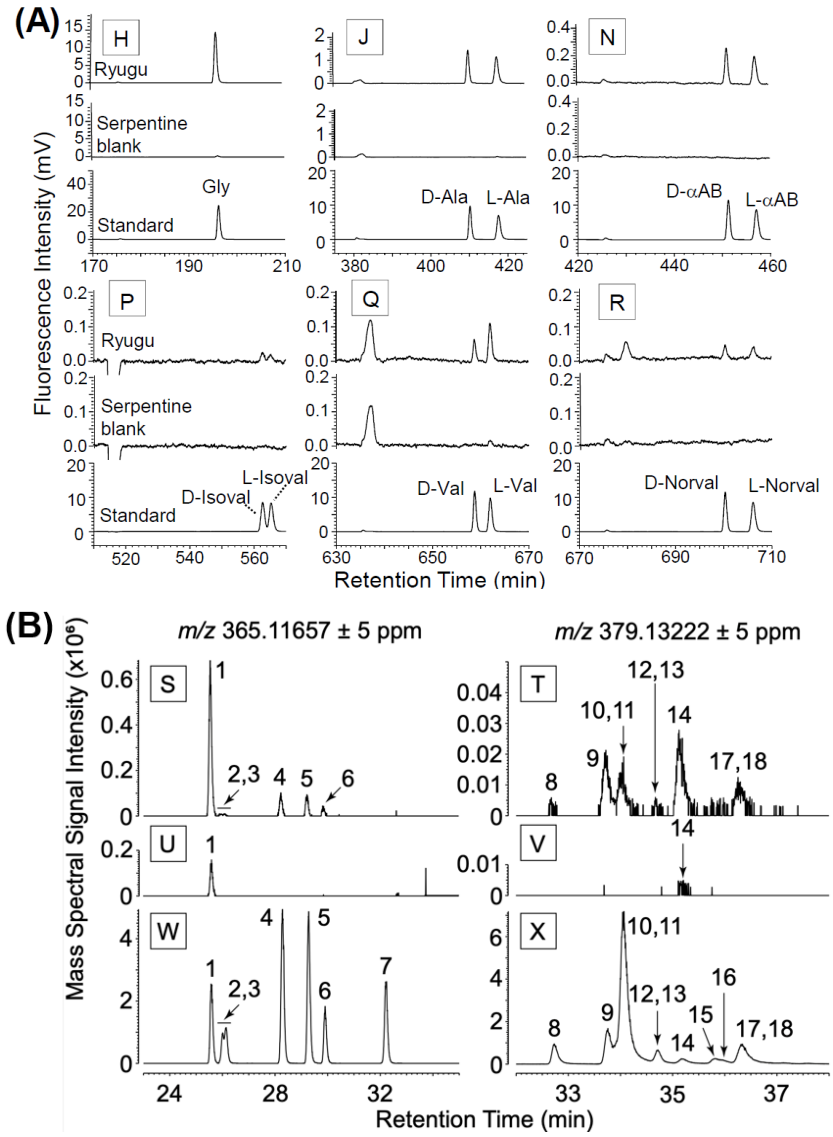

Fig. 3. Amino acids detected in the hydrolyzed hot water extract of the Ryugu sample. (A) Partial chromatograms obtained by 3D-HPLC/FD for glycine (Gly) (H), alanine (Ala) (J), α-amino-*n*-butyric acid (αAB) (N), isovaline (Isoval) (P), valine (Val) (Q), and norvaline (Norval) (R). In each panel, the Ryugu extract (top traces) is compared with baked serpentine blanks (middle traces) and terrestrial standards (lower traces). (B) Ion-extracted chromatograms from LC-FD/HRMS analysis of Ryugu sample (S and T), a serpentine blank (U and V), and mixed amino acid standards (W and X). Amino acids composed of 4 and 5 carbon atoms were detected in the Ryugu sample. Peak identifications are: 1) ɣ-amino-*n*-butyric acid, 2) D-β-amino-isobutyric acid, 3) L-β-amino-isobutyric acid, 4) D-β-amino-*n*-butyric acid, 5) L-β-amino-*n*-butyric acid, 6) α-amino-isobutyric acid, 7) D,L-α-amino-*n*-butyric acid, 8) 3-amino-2,2-dimethylbutyric acid, 9) ɣ-amino-*n*-valeric acid, 10) 3-amino-2-methylbutyric acid, 11) 4-amino-3-methylbutyric acid, 12) 3-amino-2-methylbutyric acid, 13) R-3-amino-2-ethylpropanoic acid, 14) δ-amino-*n*-valeric acid, 15) L-4-amino-2-methylbutyric acid, 16) D-4-amino-2-methylbutyric acid, 17) ɣ-amino-*n*-valeric acid, 18) 3-amino-3-methylbutyric acid.

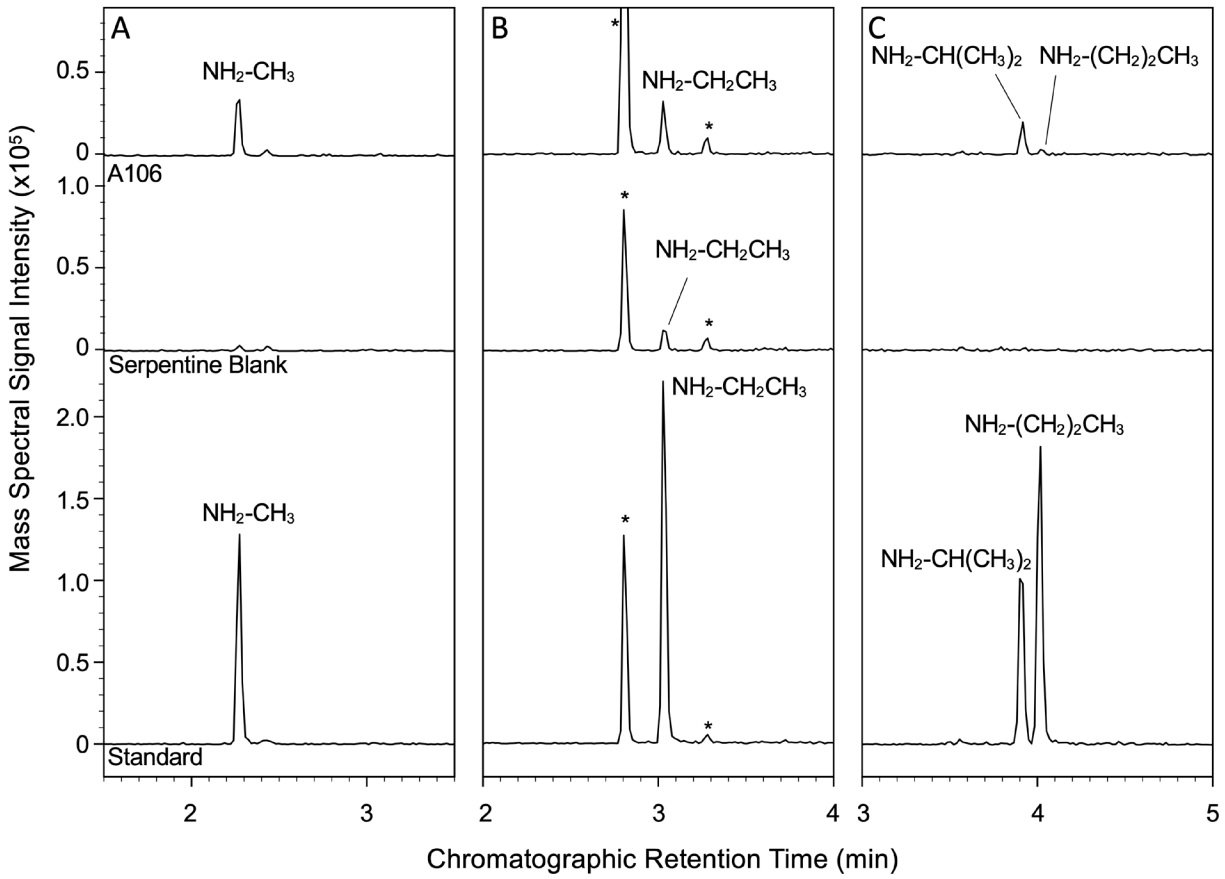

Fig. 4. Aliphatic amines in the hot water extract of Ryugu. Chromatograms measured using LC-FD/ToFMS for (A) methylamine, (B) ethylamine, and (C) n-propylamine and iso-propylamine. In each panel, the Ryugu sample (upper trace) is compared with a baked serpentine blank (middle trace) and terrestrial standards (lower trace). Asterisks indicate peaks introduced by the reagent used for derivatization.

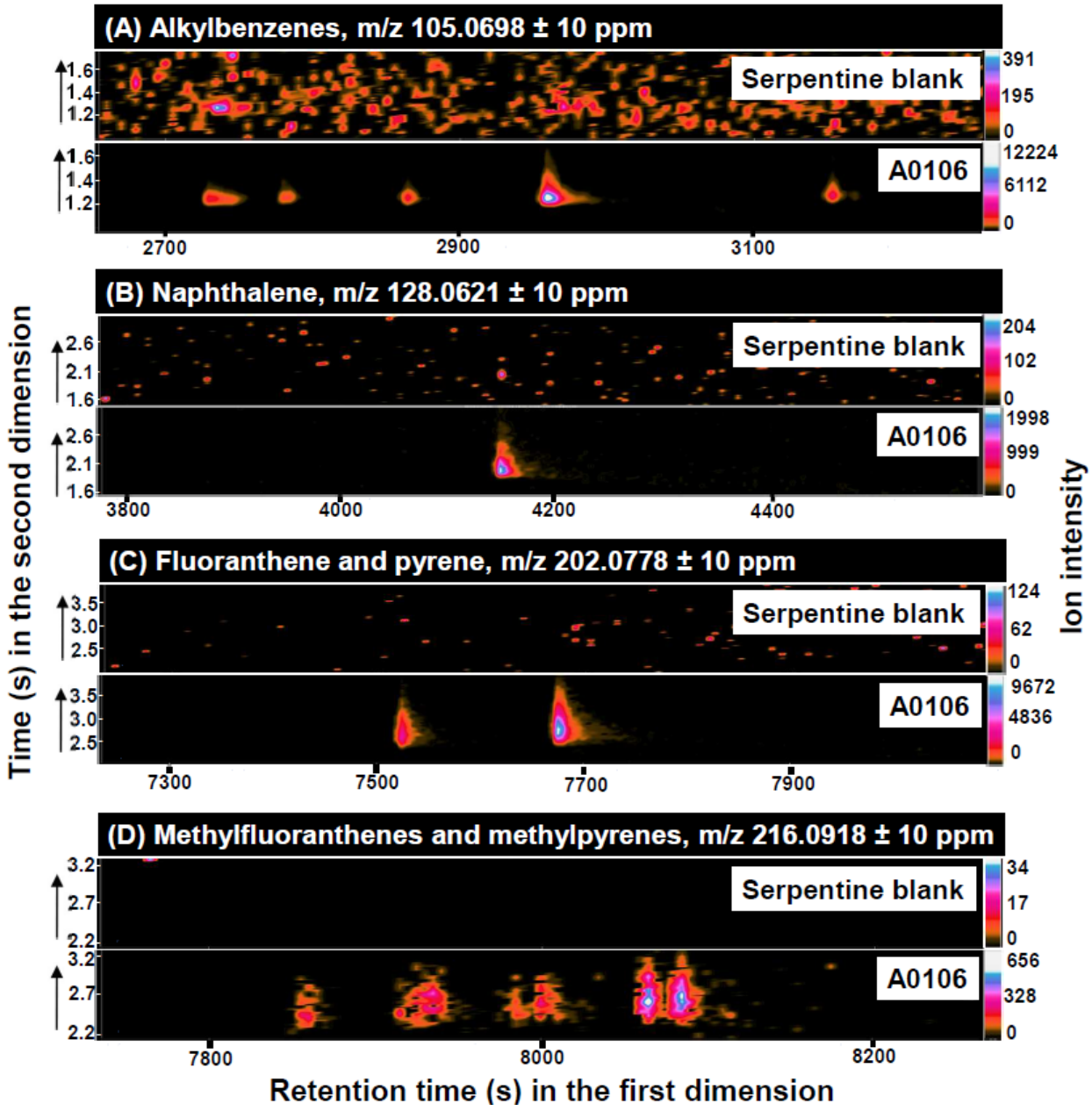

Fig. 5. Aromatic hydrocarbons in the Ryugu extract. Data were measured using GC×GC-TOFMS. (A) alkylbenzenes in the hexane extract (*m*/*z* = 105.0698), (B) naphthalene (*m*/*z* = 128.0621) in the DCM extract, (C) fluoranthene (~7520 s) and pyrene (~7680 s) (*m*/*z* = 202.0778) in the DCM extract, (D) methylfluoranthenes and methylpyrenes (*m*/*z* = 216.0918) in the DCM extract. In each panel, the Ryugu sample (lower) is compared with a baked serpentine blank (upper). Colors indicate concentration, as indicated on the color bar.

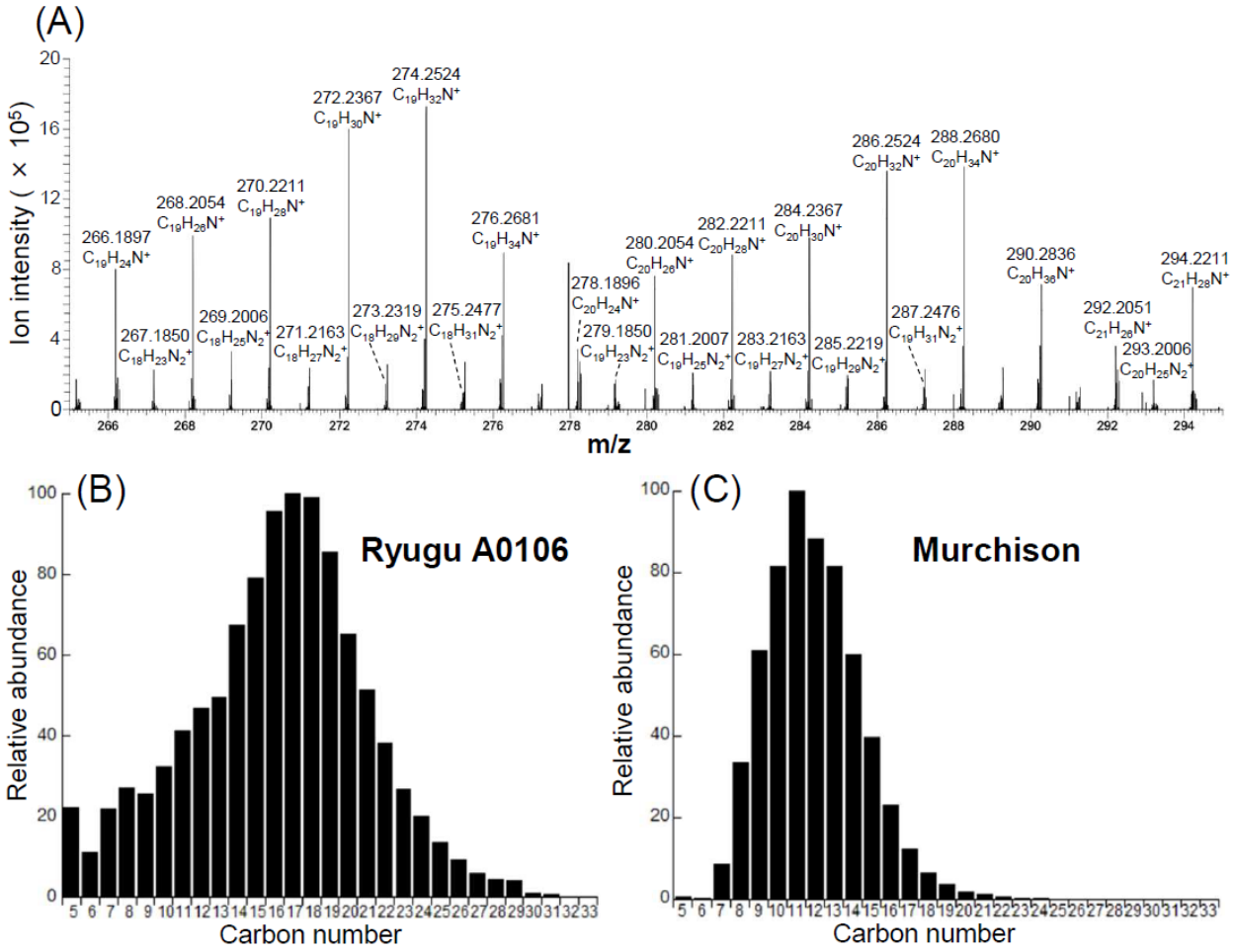

Fig. 6. CHN compounds in the methanol extract determined using nanoLC/high resolution mass spectrometry. (A) Example region of the mass spectrum of the A0106 sample *(74)*, with peaks assigned to $C_nH_{2n-16}N^+$, $C_nH_{2n-14}N^+$, $C_nH_{2n-12}N^+$, $C_nH_{2n-10}N^+$, $C_nH_{2n-8}N^+$, $C_nH_{2n-6}N^+$, $C_nH_{2n-4}N^+$, $C_nH_{2n-15}N_2^+$, $C_nH_{2n-13}N_2^+$, $C_nH_{2n-11}N_2^+$, $C_nH_{2n-9}N_2^+$ and $C_nH_{2n-7}N_2^+$ (where C_n is the carbon number). (B-C) Histograms showing the relative abundances of $C_nH_{2n-4}N^+$ (alkylpyridines) as a function of carbon number, for Ryugu (panel B) and Murchison *(11)* (panel C). Abundances are normalized to a peak value of 100. The Ryugu distribution peaks at higher carbon number than Murchison.

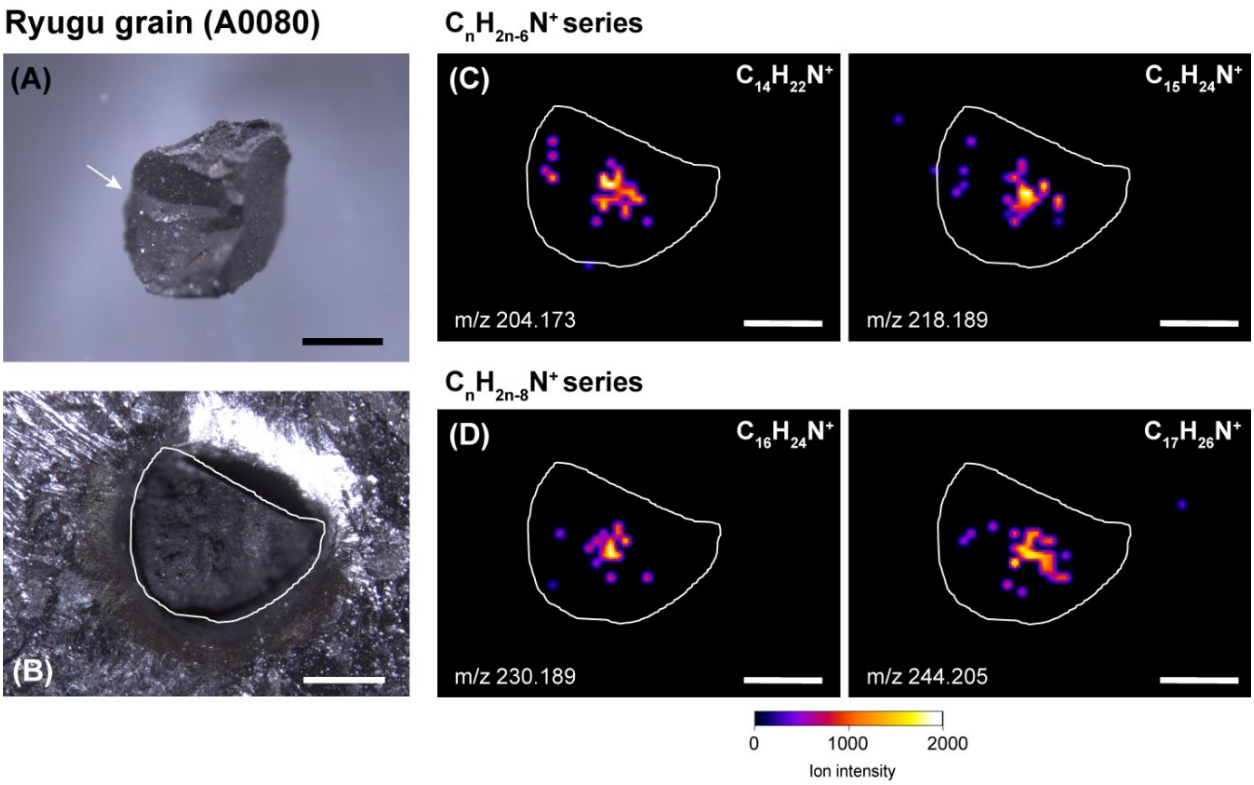

Fig. 7. Spatial distribution of CHN compounds on the surface of Ryugu grain A0080. Optical images (A) before sample preparation and (B) after embedding in an alloy. A white arrow in panel A indicates the grain surface embedded in panel B. Maps of organic molecule distribution were measured by DESI coupled with HRMS, for (C) $C_nH_{2n-6}N^+$ series (n =14, 15) and (D) $C_nH_{2n-8}N^+$ series (n =16, 17) molecules. White outlines indicate the boundary between the A0080 grain and the surrounding metal. All scale bars are 500 μm.

Supplementary Materials for

Soluble organic molecules in samples of the carbonaceous asteroid (162173) from Ryugu

H. Naraoka et al.

*Corresponding author: H. Naraoka, naraoka@geo.kyushu-u.ac.jp

DOI: 10.1126/science.abn9033

This PDF file includes:

Materials and Methods

Sample

An aggregate sample of Ryugu grains (A0106) and a single grain (A0080) were allocated to the SOM (Soluble Organic Molecules) team for the initial analysis of Hayabusa2 samples. Each sample was transported from the JAXA Extraterrestrial Samples Curation Center in Sagamihara, Japan, via a facility-to-facility transfer container (*73*) to Kyushu University (KU) for extraction and distribution. The A0106 sample consisted mainly of particles smaller than 1 mm in diameter (Fig. S1). We used the A0106 sample to analyze SOM after solvent extractions (Fig. S2). The A0106 sample was investigated spectroscopically in the near infrared wavelength range prior to the solvent extractions (*9*). The spectra indicated that the sample has a mineralogy consistent with that observed for other aggregate samples of Ryugu (*9*). We determined elemental compositions of SOM in various solvent extracts by non-target analysis using Fourier transform ion cyclotron mass spectrometry (FT/ICR-MS), and performed chromatographic molecular analyses of amino acids, aliphatic amines, carboxylic acids, aromatic hydrocarbons, and N-containing heterocyclic compounds (Fig. S2). A part of the A0106 sample was used for elemental and isotopic analyses of total carbon (C), hydrogen (H), nitrogen (N), sulfur (S), as well as pyrolyzable oxygen (O) (Fig. S2). The A0080 sample was a ~1 mm-sized grain (Fig. 7A), which was investigated for spatial SOM distribution on the sample surface by in situ analysis (Fig. S2). Other supplementary data are provided at (*74*).

CNHOS contents and their isotopic compositions

Elemental and isotopic analysis of C, N, S, H, and pyrolyzable O was performed in triplicate using elemental analyzers connected to isotope ratio mass spectrometers (EA/IRMS). For the total C, N, and S contents with their isotopic compositions ($\delta^{13}C$, $\delta^{15}N$, and $\delta^{34}S$, respectively), we used an EA/IRMS system (Flash EA1112 elemental analyzer/Conflo III interface/Delta Plus XP isotope-ratio mass spectrometer, Thermo Finnigan Co., Bremen) at Japan Agency for Marine-Earth Science and Technology (JAMSTEC) at Yokosuka. The analytical validations using the nano-EA/IRMS system were performed during rehearsal analyses and studies of the carbonaceous chondrites (*75-77*). For the total H and pyrolyzable O with their isotopic compositions (δD and $\delta^{18}O$, respectively), we used another EA/IRMS system (Elemental Analyzer/Thermal Conversion (EA/TC) coupled with Delta Plus XL isotope-ratio mass spectrometer through a Conflo III interface, Thermo Finnigan Co., Bremen) at KU (*52,78*). The δ values of the Ryugu samples for C, N, H, S, and O isotopic compositions are denoted using the international isotope standards as follows:

$\delta^{13}C = [(^{13}C/^{12}C)_{Ryugu}/(^{13}C/^{12}C)_{VPDB} - 1] \times 1000$ (‰)
using the Vienna Peedee Belemnite (VPDB) standard

$\delta^{15}N = [(^{15}N/^{14}N)_{Ryugu}/(^{15}N/^{14}N)_{Air} - 1] \times 1000$ (‰)
using Earth atmospheric nitrogen (Air) standard

$\delta D = [(D/H)_{Ryugu}/(D/H)_{VSMOW} - 1] \times 1000$ (‰)
using the Vienna Standard Mean Ocean Water (VSMOW) standard

$\delta^{34}S = [(^{34}S/^{32}S)_{Ryugu}/(^{34}S/^{32}S)_{VCDT} - 1] \times 1000$ (‰)
using the Vienna Canyon Diablo Troilite (VCDT) standard

$\delta^{18}O = [(^{18}O/^{16}O)_{Ryugu}/(^{18}O/^{16}O)_{VSMOW} - 1] \times 1000$ (‰)
using the VSMOW standard; respectively.

The CNHOS contents (wt. %) and their isotopic compositions of the Ryugu sample A0106 are shown in Table S1. The $\delta^{13}C-\delta^{15}N-\delta D$ values are plotted in Fig. 1E and 1F with those reported for various type of carbonaceous chondrites (Table S2, *13, 79-94*). The isotopic compositions have been used for classification and origins of meteorites with respect to the solar system formation. The compiled data indicate that the Ryugu sample has isotopic characteristics more similar to those of CI-type chondrites than other carbonaceous chondrites.

Solvent extractions

The extraction and analytical measurements are summarized in Fig. S2. All extraction procedures were performed on an International Organization for Standardization (ISO) 5 (Class 100) clean bench inside an ISO 6 (Class 1000) clean room at KU. All glassware used were baked in an oven at 500°C for 3 h prior to analysis to remove organic contaminants. The aggregate sample of A0106 (17.15 mg) was extracted sequentially with hexane (Hexane 5000, FUJIFILM Wako, 200 µL × 3), dichloromethane (DCM, Dichloromethane 5000, FUJIFILM Wako, 200 µL × 3), methanol (MeOH, QTOFMS grade, FUJIFILM Wako, 200 µL × 3) and H_2O (200 µL × 3, TAMAPURE-AA, Tama Chemicals C., Ltd.) using a sonicator (15 min each, Bransonic Model 1210) in a 1.5 mL polytetrafluoroethylene (PTFE, Teflon) vial followed by centrifugation (12,000 rpm × 5 min for the hexane, DCM and MeOH extractions and 14,000 rpm × 8 min for the H_2O extraction). Each combined solution (600 µL) was mixed by shaking, then divided and distributed as 200 µL (Helmholtz Center in Munich), 200µL (Goddard Space Flight Center, GSFC) and 200 µL (KU). Baked serpentine powder (17.58 mg, 500°C for 3 h) was also analyzed as a procedural blank.

A separate aggregate sample of A0106 (13.08 mg) was subjected to the hot water (200 µL) extraction at 105°C for 20 h in an N_2 purged and sealed glass ampoule. After the extraction, the content was transferred from the ampoule to a glass vial. The glass vial was centrifuged for 8 min at 14,000 rpm, then the supernatant was transferred to another sample extract vial. The glass ampoule was rinsed with 200 µL H_2O, then the H_2O solution was transferred to the residue-containing vial, which was further mixed by shaking. The glass vial was centrifuged for 8 min at 14,000 rpm, then the supernatant was transferred to the sample extract vial. This step was repeated, then the combined 600 µL solution was mixed well by shaking. The hot water extract was split into 250 µL (KU) and 250 µL (GSFC) for amino acid analysis, and 100 µL (JAMSTEC) for other analysis. The amino acid analyses were performed at KU and GSFC. Baked serpentine powder (16.21 mg, 500°C for 3 h) was also analyzed as a procedural blank.

Fourier transform ion cyclotron mass spectrometry (FT/ICR-MS)

The mass analysis was conducted with a BRUKER Solarix 12 Tesla instrument installed at the Helmholtz Center in Munich following standard operation procedure (*16*). The 100 µL MeOH extract was diluted four times and directly injected with a Hamilton syringe using a syringe pump at flow rates of 120 µL h^{-1} and 500 µL h^{-1} in electrospray ionization (ESI) and atmospheric pressure photoionization (APPI), respectively. In ESI(-), 3000 scans were accumulated for

negatively-charged ions, and 1000 scans in ESI(+) and 300 scans in APPI(+) were accumulated for positively-charged ions.

To maintain mass accuracy, performed internal calibrations on arginine clusters prior to any analysis. Relative *m/z* errors were lower 100 ppb across a range of 92 < *m/z* < 1,000. The average mass resolving power was about 400,000 at nominal mass 400. Data were internally calibrated to produce *m/z* lists and processed using the formula annotation pipeline after mass difference network analysis (*95*). The mass spectra of ESI(-) measurement are shown in Fig. 2A. The elemental compositions of molecules obtained by ESI(-), ESI(+), and APPI(+) measurements are shown in Fig. 2B and 2C. The data files are provided as Data S1 for ESI(-), Data S2 for ESI(+), and Data S3 for APPI(+) at (*74*).

Amino acid analysis

Amino acid analysis was performed by two different methods at KU and at GSFC. KU performed enantiomer separation of targeted amino acids using three dimensional-high performance liquid chromatography coupled with fluorescence detection (3D-HPLC/FD). GSFC performed non-target amino acid analysis using liquid chromatography/fluorescence detection equipped with high-resolution mass spectrometry (LC/FD-HRMS).

3D-HPLC/FD amino acid analysis at KU

The detailed procedure of amino acid analysis by 3D-HPLC/FD was reported elsewhere *(96)*. The hot water extract (~200 µL) was mixed with ~6 M HCl (~200 µL, Tama Chemicals C., Ltd.) in a closed glass vial, followed by hydrolysis at 105°C for 20 h. The resulting reaction mixture was evaporated to dryness under reduced pressure. To the residue, 100 µL of water was added, and the solution was neutralized with sodium hydroxide, which was confirmed by a pH test paper. A 20 µL aliquot of the neutralized solution was mixed with 400mM sodium borate buffer (pH 8.0, 20 µL) and 100 mM 4-fluoro-7-nitro-2,1,3-benzoxadiazole in 5 µL acetonitrile (MeCN) in a light shielded glass vial. The mixed solution was heated at 60°C for 6 min, and an aqueous 2 % (volume by volume, v/v) trifluoroacetic acid (TFA) solution (55 µL) was added to stop the reaction.

An aliquot of the reaction mixture (10 µL) was then analyzed using the 3D-HPLC/FD system. Three different columns were equipped as a dimension of the 3D-HPLC system. In the first dimension, a Singularity RP18 column (1.0 mm inner diameter (i.d.) × 250 mm length) was used for the reversed-phase separation, and the target amino acids were separated by using the gradient elution of 5-25 % MeCN and 0.025 % TFA in H_2O. In the second dimension, an anion-exchange column (Singularity AX, 1.0mm i.d. × 150mm length) was equipped, and the mobile phases were mixed solutions of MeOH-MeCN (50/50, v/v) containing formic acid (FA). The FA concentrations were 0.04 % for alanine (Ala), αAB, valine (Val), and norvaline (Norval); and 0.07 % for glycine (Gly) and isovaline (Isoval). In the third dimension, tandemly connected Singularity CSP-001S columns (1.5 mm i.d. × 500 mm, total length) were used for enantiomeric separations. A mixed solution of MeOH-MeCN (90/10, v/v) containing 0.14 % FA (for Isoval) and mixed solutions of MeOH-MeCN (50/50, v/v) containing 0.20 % FA (for Ala, αAB, Val, and Norval) or 0.03 % FA (for Gly) were used as mobile phases. The N-(7-nitro-2,1,3-benzoxadiazol-4-yl)-amino acids were detected by their fluorescence emission at 530 nm with

excitation at 470 nm. The concentration of amino acid was determined by single analysis due to the sample limitation. The analytical uncertainty was estimated to be 3-8 % of the quantitative value of amino acid based on a quadruple analysis of amino acids in carbonaceous chondrites (*96*). The result of this amino acid analysis is shown in Fig. 3A and Table S3. The data file (fluorescence intensity vs. time) is provided at Data S4 (*74*).

LC-FD/HRMS amino acid analysis at GSFC

Samples were unpacked and inspected in an ISO 5 flow bench in an ISO < 8 (Class <100,000) whiteroom and then stored in a -20°C freezer until analysis. All glass materials were cleaned by rinsing in ultrapure water (Millipore Integral 10, 18.2 MΩ cm, < 3 ppb total organic carbon) then baking at 500°C in air in a muffle furnace overnight to remove residual organics. Standards and reagents were purchased from Alfa Aesar, Sigma-Aldrich, Acros Organics, Mann Research Laboratories, and Thermo Scientific and used without further purification except as noted below. HPLC-grade DCM, semiconductor-grade NaOH, ultrapure 6 M HCl (Tama Chemicals Co., Ltd.) were used during sample preparation. Functionalized aminopropyl silica gel was from SiliCycle (SiliaBond, 40-63 µm particle size) and cleaned using MeOH and DCM followed by drying under vacuum. The AccQ•Tag reagent and solvents used during amine analysis were from Waters.

Samples from hot water extract (80 µL each) as well as a serpentine and procedural blank were each mixed with 8 µL of 1.5 M doubly distilled (dd) HCl before being dried under vacuum and then acid hydrolyzed under 6 M ddHCl vapor at 150°C for 3 h (*96*). The 6 M ddHCl that was used for acid vapor hydrolysis was ultrapure 6 M HCl (Tama Chemicals C., Ltd.) that was doubly distilled prior to use with these samples. Following acid hydrolysis, retrieved test tubes were dried under vacuum to remove HCl. Test tubes were then rehydrated with 100 µL of ultrapure water and transferred into separate, capped derivatization vials. Each sample and blank test tube subsequently underwent two successive 100 µL rinses using ultrapure water, which were individually transferred to their respective derivatization vials. The resultant 300 µL solution in each sample and blank derivatization vial was then dried under vacuum to ensure full removal of residual HCl from the acid vapor hydrolysis process. The residues in the derivatization vials were then each reconstituted in 20 µL of a 0.1 M sodium borate solution and dried again under vacuum. Finally, each derivatization vial was resuspended with 20 µL of ultrapure water and derivatized with 5 µL of *o*-phthaldialdehyde/*N*-acetyl-L-cysteine (OPA/NAC) for 15 min at room temperature (~21°C). OPA/NAC derivatization added a fluorescent tag to the primary amino group and results in a diastereomer for separation of D- and L-amino acid enantiomers by liquid chromatography. The derivatization reaction was then quenched with 75 µL of 0.1 M dd hydrazine hydrate, at which point, the solutions were promptly injected into the LC-FD/HRMS system for amino acid analysis.

Amino acids were analyzed by LC-FD/HRMS using a Vanquish Horizon LC (Thermo Fisher Scientific) coupled to a Vanquish fluorescence detector (Thermo Fischer Scientific), and a Q Exactive hybrid quadrupole-Orbitrap mass spectrometer (Thermo Fisher Scientific). Compound identifications were determined by chromatographic retention time, optical fluorescence, and accurate mass measurements based on comparison to a mixed amino acid standard. A mass precision of 3 ppm, defined as [(measured m/z)–(calculated m/z)](calculated m/z)$^{-1}$]×10^6 (ppm), was implemented for mass identification of target analytes by HRMS.

Two mobile phases were used during LC analyses of 2- to 4-carbon (C_2–C_4) and 6-carbon (C_6) amino acids: a) 45 mM ammonium formate with 7 % MeOH, pH adjusted to 9.0 and b) LC-MS grade MeOH. Mobile phase a) was made by first mixing 2 mL of LC-MS grade formic acid with 1033 mL of LC-MS grade water, then titrating the solution to pH 9.0 with 1M aqueous ammonium hydroxide, and finally adding 85 mL of LC-MS grade MeOH. The 1M ammonium hydroxide solution that was used for titration was generated by diluting a 7.3 M stock solution of aqueous ammonium hydroxide (assay = 28.6 %, ammonia in water) with LC-MS grade water to a final concentration of 1 M. Two mobile phases were used during LC analyses of 5-carbon (C_5) amino acids: c) 45 mM ammonium formate with 7 % MeOH, pH adjusted to 7.4 and d) LC-MS grade MeOH. Mobile phase c) was prepared identically to mobile phase a), except mobile phase c) was titrated to pH 7.4 with 1 M aqueous ammonium hydroxide.

Chromatographic separation was achieved using a Waters ACQUITY UPLC BEH C18 VanGuard Pre-column (2.1 mm i.d. × 50 mm length, 1.7 µm particle size) in front of two stationary phases used in series: i) Waters ACQUITY UPLC CSH C18 (2.1 mm i.d. × 150 mm length, 1.7 µm particle size) and ii) Waters ACQUITY UPLC BEH Phenyl (2.1 mm i.d. × 150 mm, 1.7 µm particle size). The C_2–C_4 and C_6 amino acids were eluted using the following gradient: 0–35 min, 0-55 % eluent b, 35–45 min, 55 – 100 % eluent b, 45–50 min, isocratic at 100 % eluent b, 50–50.1 min, 100–0 % eluent b, 50.1–60 min, isocratic at 0 % eluent b. The eluent flow rate was 0.15 mL min^{-1} for the entirety of the run and columns were heated at 33°C. The autosampler was kept at a constant temperature of 5°C and the injection volume was 10 µL. The FD was operated with an excitation wavelength of 340 nm and an emission wavelength of 450 nm, and was maintained a temperature of 33°C. The LC-FD settings used to perform chromatography of the C_5 amino acids were identical to those of the C_2–C_4 and C_6 amino acids, except the C_5 amino acid chromatography required the use of a difference aqueous mobile phase and a different gradient: 0–25 min, 15–20 % eluent d, 25–25.06 min, 20–35 % eluent d, 25.06–44.5 min, 35–40 % eluent d, 44.5–45 min, 40–100 % eluent d, 45–50 min, isocratic at 100 % eluent d, 50–50.1 min, 100–15 % eluent d, 50.1–60 min, isocratic at 15 % eluent d.

For all amino acids targeted, the HRMS system utilized a heated ESI(+) source to ionize target analytes, which was operated according to the following conditions: sheath gas (N_2) flow rate = 40 arbitrary unit (a.u.), auxiliary gas (N_2) flow rate = 10 a.u., sweep gas (N_2) flow rate = 2 a.u., spray voltage = 3.50 kV, capillary temperature = 350°C, S-lens (or stacked ring ion guide) RF (radio frequency) level = 50.0 %, and auxiliary gas heater temperature = 300°C. For all amino acid analyses, the HRMS system was operated in Full MS – SIM (single ion monitoring) scan mode and implemented the following scan parameters: scan range = 150–2000 *m/z*, mass resolving power setting = 70,000 (at full-width-half-maximum for *m/z* 200), fragmentation = none, polarity = positive, microscans = 1, AGC (automatic gain control) target = 1×10^6 ions, and maximum injection time = 50 ms. The result of this amino acid analysis is shown in Fig. 3B and Table S3. The data file (*m/z* vs. time) is provided as Data S5 at (*74*).

Aliphatic amine analysis

Samples from hot water extract (10 µL each) as well as a serpentine blank derivatized with the AccQ•Tag protocol (*97*) protocol which adds a fluorescent tag to primary and secondary amines (Fig. S2). Analysis was on a Waters ACQUITY H Class UPLC with a Waters fluorescence detector and a Waters Xevo G2-XS time of flight mass spectrometer (LD-FD/TOFMS) with an

ESI(+) source (*98*). Aqueous amine standards were evaluated at five concentrations, and a linear least-square model was fit for each amine. Peak areas generated from the mass chromatogram of AccQ•Tag derivatives were used to determine the concentrations of amines. The average value of three separate measurements of the same extracted sample was determined as the abundance of each analyte. The result of this amine analysis is shown in Fig. 4 and Table S3. The data file (*m/z* vs. time) is provided as Data S6 at (*74*).

Volatile compound analysis

Samples of the hexane and DCM extracts (2 µL each) as well as procedural blanks were analyzed without derivatization via GC-QMS using a GC (Thermo Trace 13100) equipped with a 5 m base-deactivated guard column (Restek, 0.25 mm i.d.) and a PoraBOND Q (0.25 mm i.d. × 25 m length, 3 µm film thickness; Agilent) fused silica column, coupled to an electron-impact triple-quadrupole mass spectrometer (Thermo TSQ; ion source set at 250°C and 70 eV). The GC oven was programed at 130°C for 1 min, then to150°C at 50°C min^{-1}, held for 4 min, then to 300°C at 40°C min^{-1}, and held for 30 min. Ultrahigh purity He (5.0 grade) was used as carrier gas at 1.5 mL min^{-1}. Samples were injected in triplicate in split mode (split flow: 50 mL min^{-1}, held for 5 min under constant flow) in aliquots of 1 µL. Mass spectra were used to identify compounds by comparison to reference standards, detection limits are estimated to be <1 pmol in solution. The result of this volatile compound analysis is shown in Fig. S4. The data file (*m/z* vs. time) is provided as Data S7 at (*74*).

Monocarboxylic acid analysis

Samples from the hot water extract (50 µL each) as well as a procedural blank were analyzed for carboxylic acids by GC-QMS. Briefly, the samples were acidified using 10 µL 2 M NaOH, dried under vacuum overnight, then the samples were suspended in 50 µL of 6 M HCl, 30 µL of 2-pentanol, 200 µL of DCM, and heated at 100°C for 16 h in sealed PTFE-lined screw cap vials in a heating block. The derivatized samples at room temperature were passed through a short column of aminopropyl silica gel (5 mm i.d. × 45 mm length), followed by two DCM rinses (~3 mL each time), and N_2-gas blow-drying. The derivatized carboxylic acids were re-dissolved in 80 µL of DCM and analyzed using a gas chromatographer (Thermo Trace 13100) equipped with a 5 m base-deactivated fused silica guard column (Restek, 0.25 mm i.d.), two Rxi-5ms (0.25 mm i.d. × 30 m length × 0.5 µm film thickness; capillary columns connected in series using SilTite µ-unions by Restek), and coupled to an electron-impact triple-quadrupole mass spectrometer (Thermo TSQ, ion source set at 250°C and 70 eV). The GC oven was programed as follows: initial temperature held at 40°C for 1 min, then to 110°C at 15°C min^{-1}, then to 140°C at 10°C min^{-1}, and finally to 300°C at 30°C min^{-1} with a final hold of 5 min. We used ultrahigh purity He (5.0 grade) as carrier gas at 4.7 mL min^{-1}. Aliquots of 1 µL injections of the derivatives were made in triplicated in split mode (split flow: 5 mL min^{-1}, held for 5 min under constant flow). The identification and quantification of the derivatized carboxylic acids were performed by comparison to reference standards and calibration curves following published methods (*36, 98*). The result of this monocarboxylic acid analysis is shown in Fig. S5 and Table S4. The data file (*m/z* vs. time) is provided as Data S8 at (*74*).

Aromatic hydrocarbon analysis

Samples of the hexane, DCM, MeOH, and DCM/MeOH extracts as well as procedural blanks were analyzed without derivatization using an Agilent 7890B gas chromatograph coupled to a LECO Pegasus HRT+4D time of flight mass spectrometer (ion source set at 250°C and 70 eV; GC×GC-TOFMS). The GC oven was equipped with a 5 m base-deactivated fused silica guard column (Restek, 0.25 mm i.d.) and two Rxi-5ms (0.25 mm i.d. × 30 m length, 0.5 µm film thickness; capillary columns connected in series using SilTite µ-union connectors, Restek). The temperature of the primary column was held at 40 °C for 10 min, then increased to 60°C at 1°C min^{-1}, held for 5 min at 60°C, then increased to 110°C at 2°C min^{-1}, held for 5 min at 110°C, then increased to 260°C at 2°C min^{-1}, held for 5 min at 260°C, finally increased to 280°C at 20°Cmin^{-1} and held for 25 min at 280°C. The secondary oven offset temperature was kept at 5°C relative to the primary oven, the modulation temperature offset was kept at 15°C, and a modulation period of 5 s was applied. The carrier gas used was ultrahigh purity grade helium (5.0 grade) at 1.4 mL min^{-1}. Duplicate injections of samples were made in splitless mode in aliquots of 2 µL. Data were processed using the LECO Corp. ChromaTOF software. Mass spectra were used to identify compounds by comparison to reference standards were possible, detection limits are estimated to be ~1 pmol in solution. The result of this aromatic hydrocarbon analysis is shown in Fig. 5. The data file (*m/z* vs. time) is provided as Data S9 at (*74*).

N-containing heterocyclic compound analysis

Sample solution (1 µL) of the MeOH extract was analyzed using a nano liquid chromatograph (UltiMate 3000 RSLCnano, Thermo Fisher Scientific) coupled with a high-resolution mass spectrometer (HRMS, Q-Exactive Plus, Thermo Fisher Scientific) equipped with a nano ESI(+) ion source (*100*), using a nano amide column (Accucore Amide, 75 µm i.d. × 150 mm length, Thermo Fisher Scientific). The eluent mixture of a (2 mM $HCOONH_4$, which was prepared from LCMS grade 1 M $HCOONH_4$ diluted with QTOFMS grade H_2O, FUJIFILM Wako) and b (MeCN, QTOFMS grade, FUJIFILM Wako) was used at a flow rate of 250 nL min^{-1}, where the ratio a/b stayed at 1/99 in the first 12 min, then programmed by a linear gradient from 1/99 to 35/65 in 10 min, followed by at 35/65 for 8 min. The ESI(+) voltage and capillary temperature were set to 1.8 kV and 250°C, respectively. The positive ions were measured by a full scan mode over a range of *m/z* 62 to 500 with a mass resolving power setting of 140,000 (at full-width-half-maximum for *m/z* 200). The maximum injection time and the AGC target were set to 50 ms and 1×10^6 ions, respectively. Most ions were observed as a protonated form of the molecular mass (M) as $[M + H]^+$. A lock mass mode was used to calibrate the mass using protonated dioctyl phthalate ($[C_{24}H_{38}O_4 + H]^+$ = 391.28429 Da), which was derived from the tubing or solvents. The lock-mass measurement gave a mass precision of less than 3 ppm. The acquired mass spectral signal was analyzed by the Xcalibur software (Thermo Fisher Scientific). The MeOH extract of the Murchison grains (5.44 mg) was also analyzed for a comparison. A mass spectrum (*m/z* 265-295) of the A0106 MeOH extract is shown in Fig. 6A. The data of full mass spectrum (*m/z* vs. time) is provided as Data 10 at (*74*). The chromatographic data of $C_nH_{2n-4}N$ molecules from the MeOH extracts A0106 and Murchison samples are shown in Table S5.

Organic molecular imaging by in-situ analysis

An about 1 mm-sized Ryugu grain (A0080) was embedded in a soft eutectic alloy (U-alloy eutectic point of 46.7°C; U-47, Osaka Asahi Co., Ltd) because of the expected fragility of Ryugu samples. No blazing or polishing was performed on the sample surface. Imaging of organic molecules was performed by in-situ analysis using a two-dimensional desorption electrospray ionization (DESI) ion source (Omni Spray Source 2D, Prosolia Inc.) equipped with an HRMS (Q-Exactive Plus, Thermo Scientific) in an ISO 5 clean room at KU. The electrically-charged MeOH (QTOFMS grade, FUJIFILM Wako) was used as a spray solvent at a rate of 3 μL min^{-1}, and the electrospray voltage was set to 3 kV. The DESI emitter was mounted about 100 μm above from the sample surface and arranged at an angle of 55º with respect to the surface. The pressure of nebulizer N_2 gas was set to 0.7 MPa. The desorbed ions were collected at the moving sample surface beneath the spray. The imaging was performed using a motorized x–y stage by continuously scanning the sample surface in the x-direction with a rate of 55 μm s^{-1}. The y-direction was stepped in 50 μm increments. The positive ions were measured over *m/z* 50−500 range using a full scan mode with a mass resolving power of 140,000 (at full-width-half-maximum for *m/z* 200). The maximum injection time and the AGC target were set to 200 ms and 5×10^6 ions, respectively. The obtained mass spectral data file was converted into Analyze 7.5 format (3D image file: x, y, and *m/z*) using FireFly software (Prosolia Inc.) and then imported to BioMap (*101*) for visualization. The apparent mass resolution of the constructed DESI images was 0.001 Da. A baked antigorite grain (~2 × 0.5 mm) embedded in a U-47 alloy was also analyzed under the same condition as a blank, showing no mass peaks detected in Fig. 7 (Fig. S8). The obtained DESI images are shown in Fig. 7C-D for the Ryugu sample and in Fig. S8 for a serpentine blank. The data file of mass spectrum (*m/z* vs. ion intensity) on the sample surface is provided as Data S11 at (*74*).

FTIR measurement of the solvent extract

FTIR measurement of the solvent extracts was performed using a Nicolet iN10 infrared microscope (Thermo Fisher Scientific) in an ISO 6 clean room at KU. Solvent extract (1-2 μL) was dropped onto a BaF_2 plate (1 mm thick) and dried in air on an ISO 5 clean bench. Transmission spectra acquired using a mercury–cadmium–telluride detector at liquid N_2 temperature with an aperture size of 300 × 300 μm. The microscope and detector were continuously purged with dry N_2 gas during analysis. Acquisitions of 256 scans were collected with a resolution of 4 cm^{-1} (2.5–94 nm) between 4000–675 cm^{-1} (2.5–15.4 μm). Background spectra were acquired with the blank BaF_2 plate. The FTIR spectra of DCM, MeOH and H_2O extracts of the Ryugu sample and blank are shown in Fig. S6A-C. The FTIR spectral data (wavenumber (cm^{-1}) −wavelength (μm) −transmittance (%)) is provided as Data S12 at (*74*).

Supplementary Text

Hexamethylenetetramine (HMT) has been detected in the aqueous extract of several carbonaceous meteorites (*59*). Since the formation of HMT on the meteorite parent bodies is not favored due to difficulties in the presence of volatile precursors such as formaldehyde and ammonia, both of which are necessary for HMT formation (*58*), the meteoritic HMT might be the remnant of photochemical reactions in the interstellar medium (*59*). Laboratory experiments

demonstrated that HMT is easily decomposed under hydrothermal conditions. When HMT is heated at 150ºC in the aqueous solution (pH = 10), it is completely decomposed within a couple of weeks (*61*). While it is heated at 100ºC for one month under the similar conditions, no decomposition was observed, even in the presence of amorphous silicates; just its hydrogen was exchanged with that of ambient water (*60*). Hence, its non-detection in any Ryugu extracts suggests that, if HMT was present at the formation of Ryugu, it may have been heated with water at temperatures above its decomposition temperature. Since N-heterocyclic molecules such as alkyl homologues of pyridines and imidazoles are formed by hydrothermal decomposition of HMT (*61*), their presence in the MeOH extract supports the above hypothesis. Note that the degree of thermal stability of HMT may vary with ambient conditions such as pH and water contents.

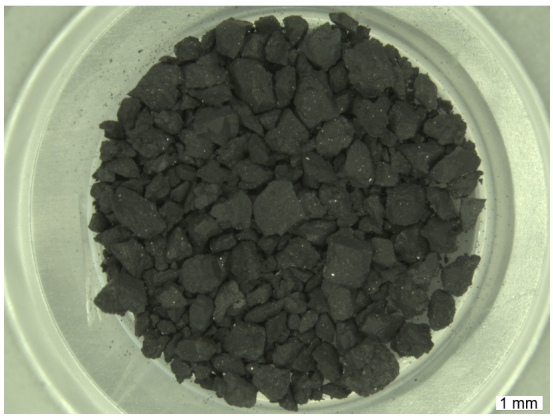

Fig. S1. An aggregate A0106 Ryugu sample. The scale bar corresponds to 1 mm. Image taken by H. Naraoka at KU.

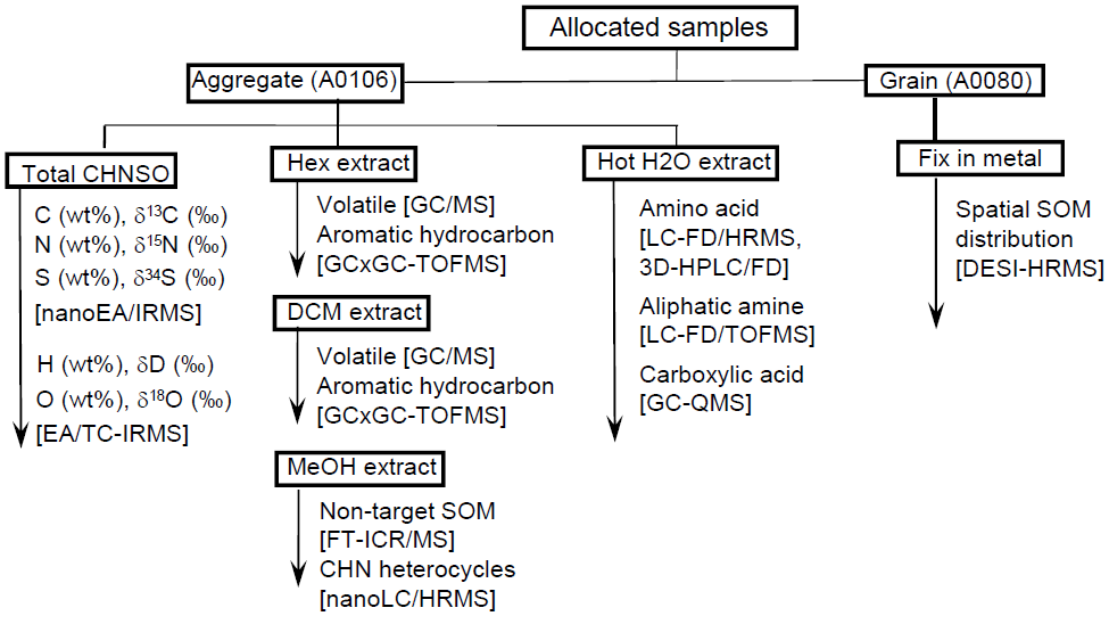

Fig. S2. Analytical scheme for Ryugu samples.

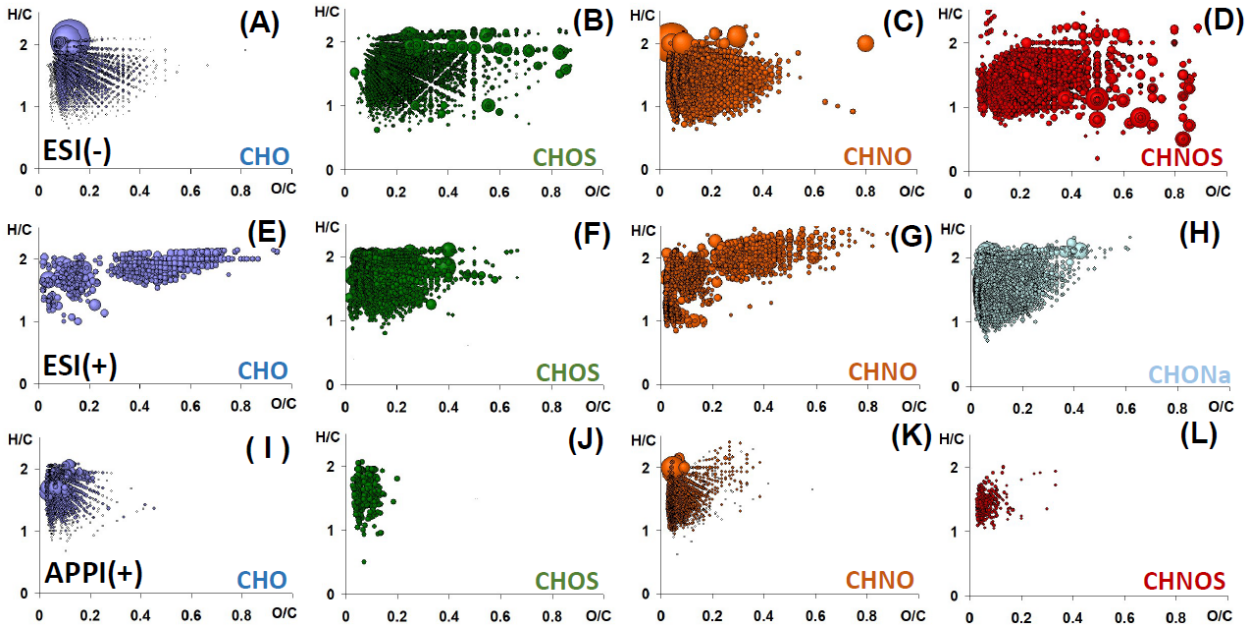

Fig. S3. O/C-H/C plots of the Ryugu extract determined by FTICR/MS. Oxygen-containing molecules were identified using ESI(-) (A-D), ESI(+) (E-H), and APPI(+) (I-L). The size of the bubble indicates the intensity of the original signals in the mass spectra. (A) CHO by ESI(-), (B) CHOS by ESI(-), (C) CHON by ESI(-), (D) CHONS by ESI(-), (E) CHO by ESI(+), (F) CHOS by ESI(+), (G) CHON by ESI(+), (H) CHONS by ESI(+), (I) CHO by APPI(+), (J) CHOS by APPI(+), (K) CHON by APPI(+), and (H) CHONS by APPI(+). The S-containing molecules by ESI(-) were highly oxygenated ((B) and (D)), indicating a diverse suite of sulfur-oxygenated organic molecules.

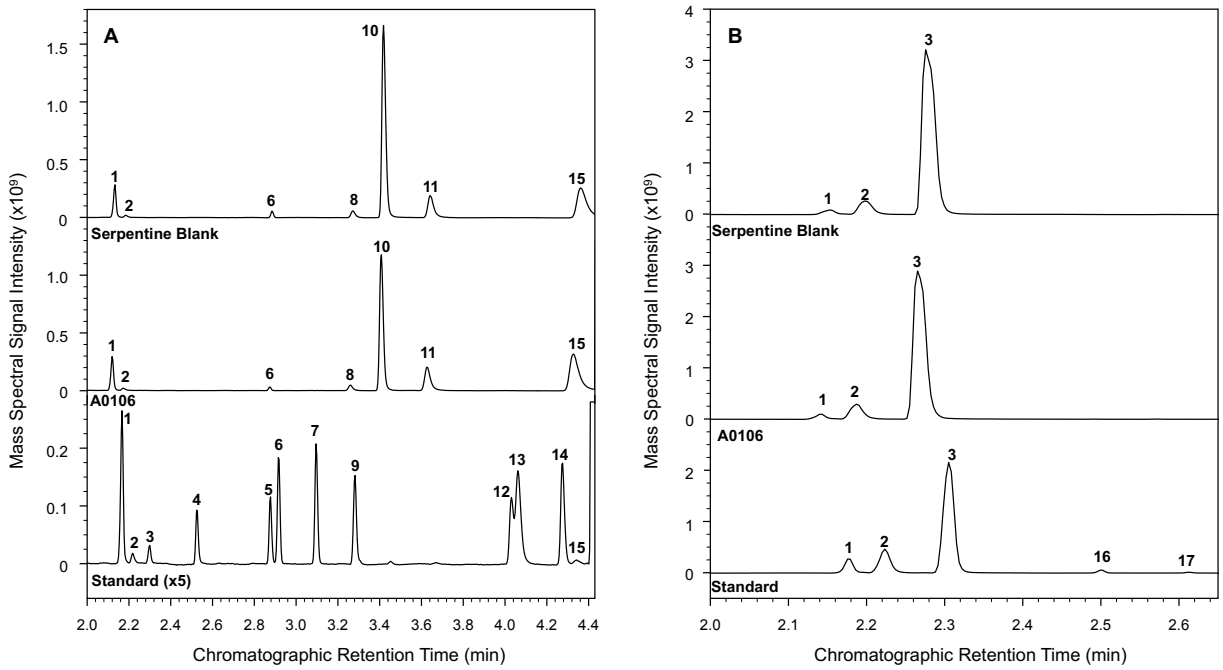

Fig. S4. GC-QMS total ion chromatograms of the hexane fraction (A) and DCM fraction (B) of sample A0106 in comparison with the serpentine blank and standards. No peaks in A0106 were seen that were not in the blank. The compound identities are: 1) nitrogen, 2) water, 3) methanol, 4) ethanol, 5) acetone, 6) DCM, 7) methyl acetate, 8) isopentane, 9) diethyl ether, 10) *n*-pentane, 11) cyclopentane, 12) methyl ethyl ketone, 13) tetrahydrofuran, 14) ethyl acetate, 15) 2,2-dimethylbutane, 16) methyl formate, and 17) acetonitrile.

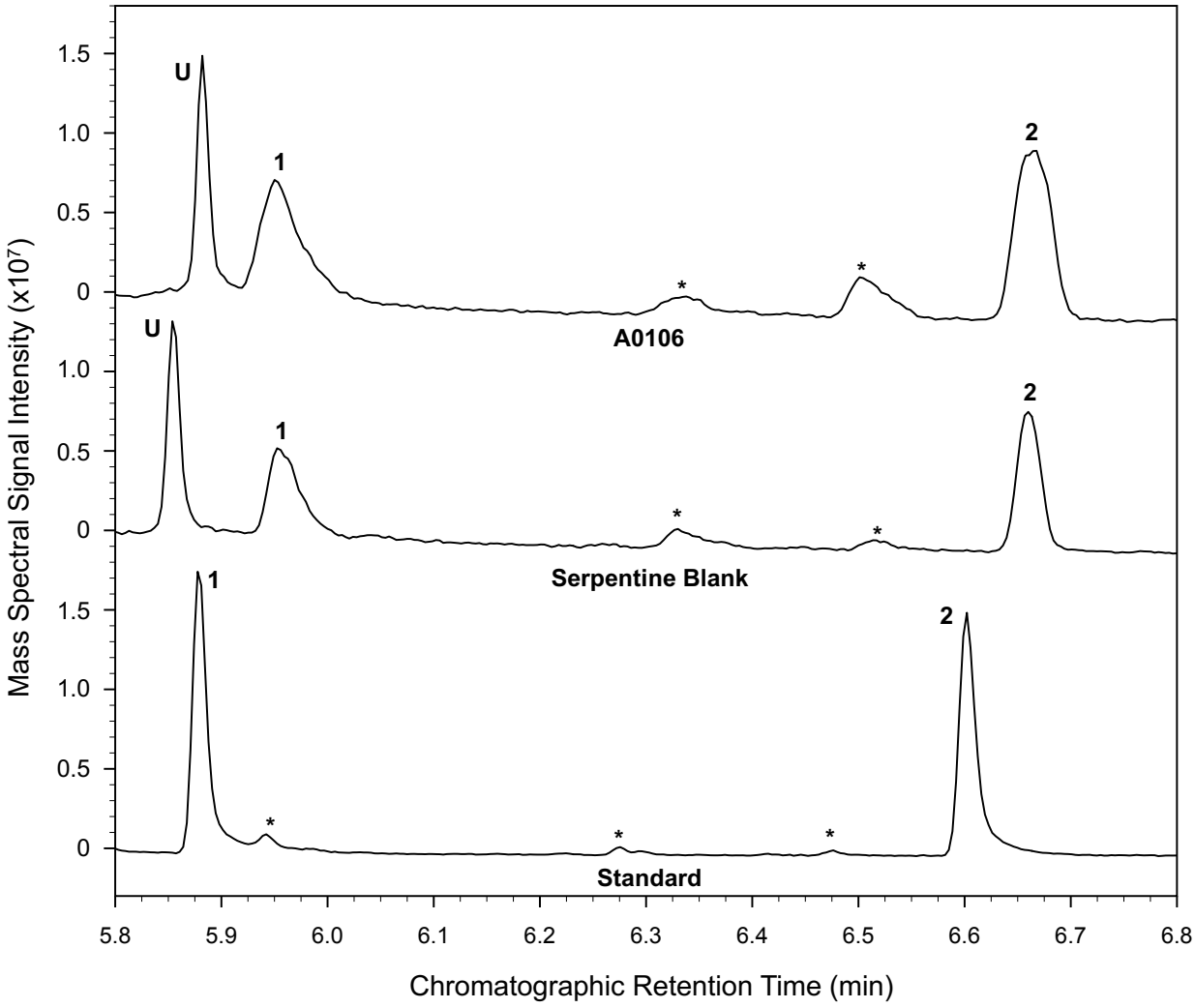

Fig. S5. Positive electron-impact GC-QMS chromatogram (5.8 – 6.8 min region, *m/z* = 70+87 ±0.5) of hot-water extracted derivatized carboxylic acids from Ryugu (A0106), procedural-serpentine blank, and commercially available standards. Identifications: 1) formic acid, 2) acetic acid, U) unknown compound. Asterisks indicate peaks introduced by the reagent used for derivatization.

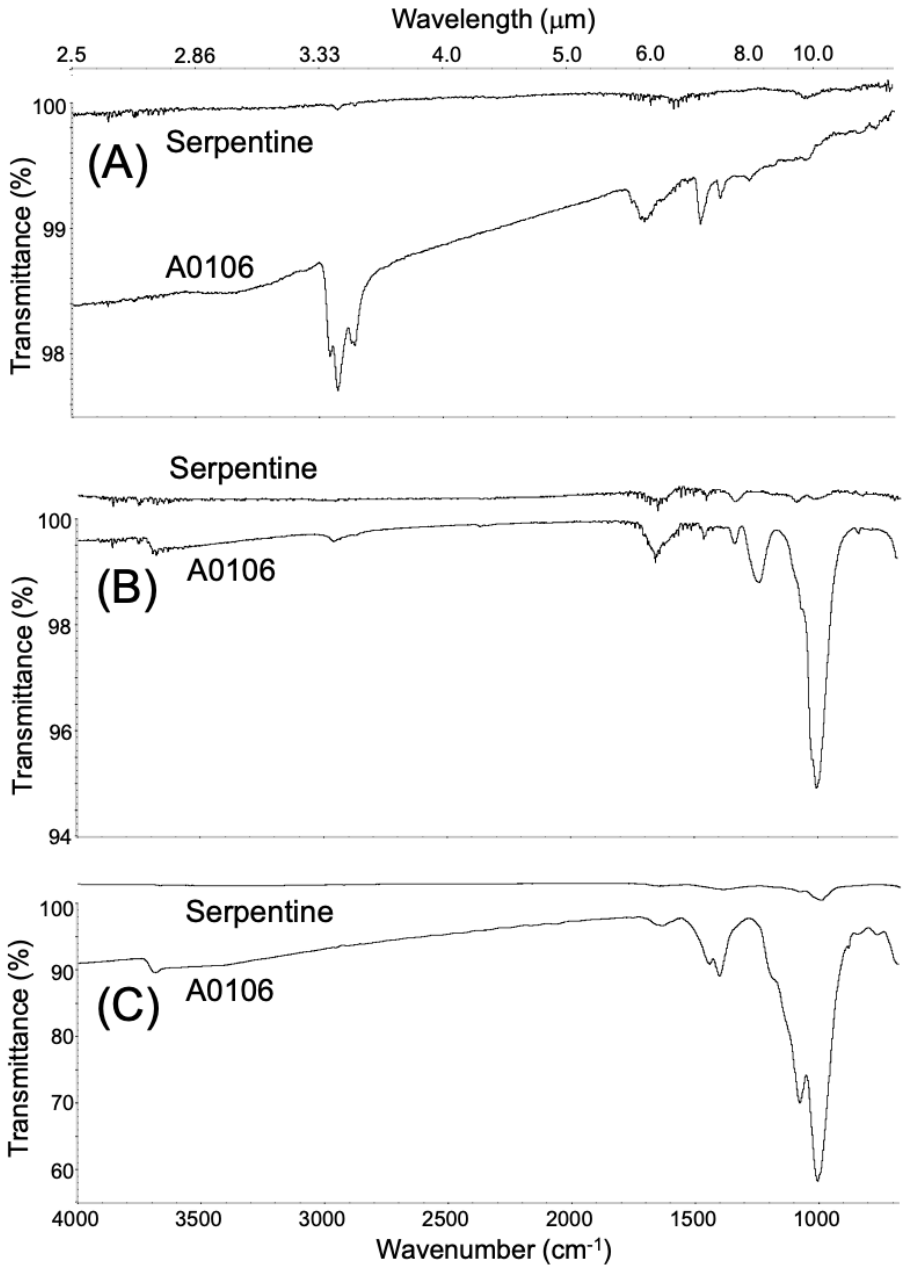

Fig. S6. FTIR spectra of the (A) DCM, (B) MeOH, and (C) H_2O extracts of the Ryugu sample (A0106) and serpentine blank. The DCM extract of A0106 exhibited an absorption at 2850-2950 cm^{-1} (3.51-3.39 μm) (CH_2/CH_3 bonds). The H_2O extract of A0106 contained very fine suspended material showing various absorption bands at 750-1650 cm^{-1} (13.3-6.1 μm) (C-H and C-C bonds) likely derived from a large PAH structure except for the strongest absorption peak at ~1000 cm^{-1} (~10 μm) (Si-O). The various absorption peaks at 750-1650 cm^{-1} (13.3-6.1 μm) regions have often been observed by the IR observations toward interstellar medium.

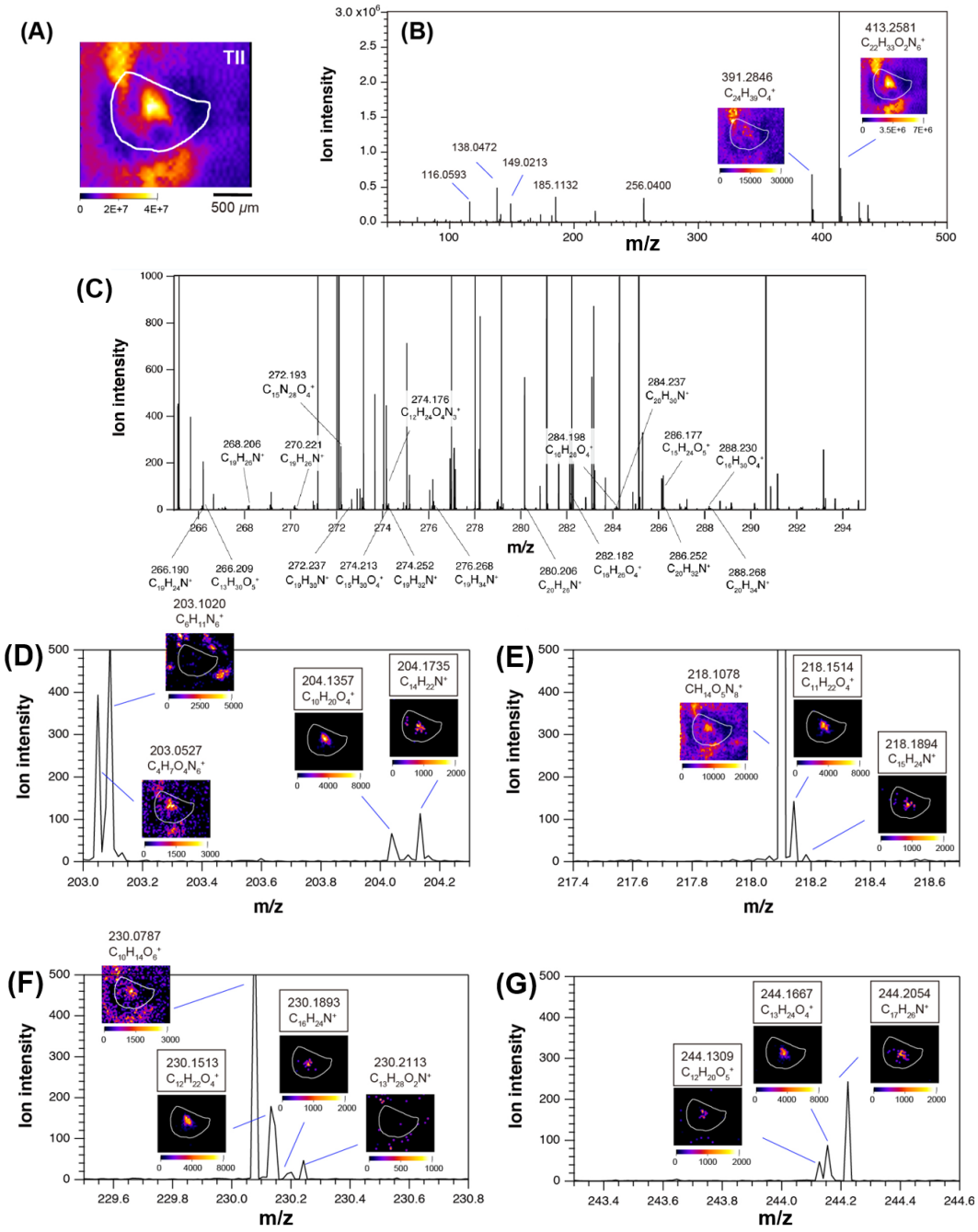

Fig. S7. DESI images and mass spectra from the A0080 surface. (A) Total ion image (TII) and (B) mass spectrum of total ion from region of interest (ROI) shown by white outline in (A). The criteria for molecule identification was [ion intensity from ROI] > [ion intensity from the surrounding metal ×10]. Many ions in the mass spectrum were derived from spray solvent, tubing, and/or surrounding air. (C) Magnified mass spectrum between *m/z* 265 to 295 in (B) for comparison to Fig. 6A. (D-G) Magnified mass spectra in (B) and DESI images corresponding for each peak including CHN compounds in Fig. 7. (D) *m/z* 203.00 to 204.25, (E) *m/z* 217.40 to 217.65, (F) *m/z* 229.55 to 230.80, and (G) *m/z* 243.35 to 244.60. The molecules in boxes are detected from the sample surface.

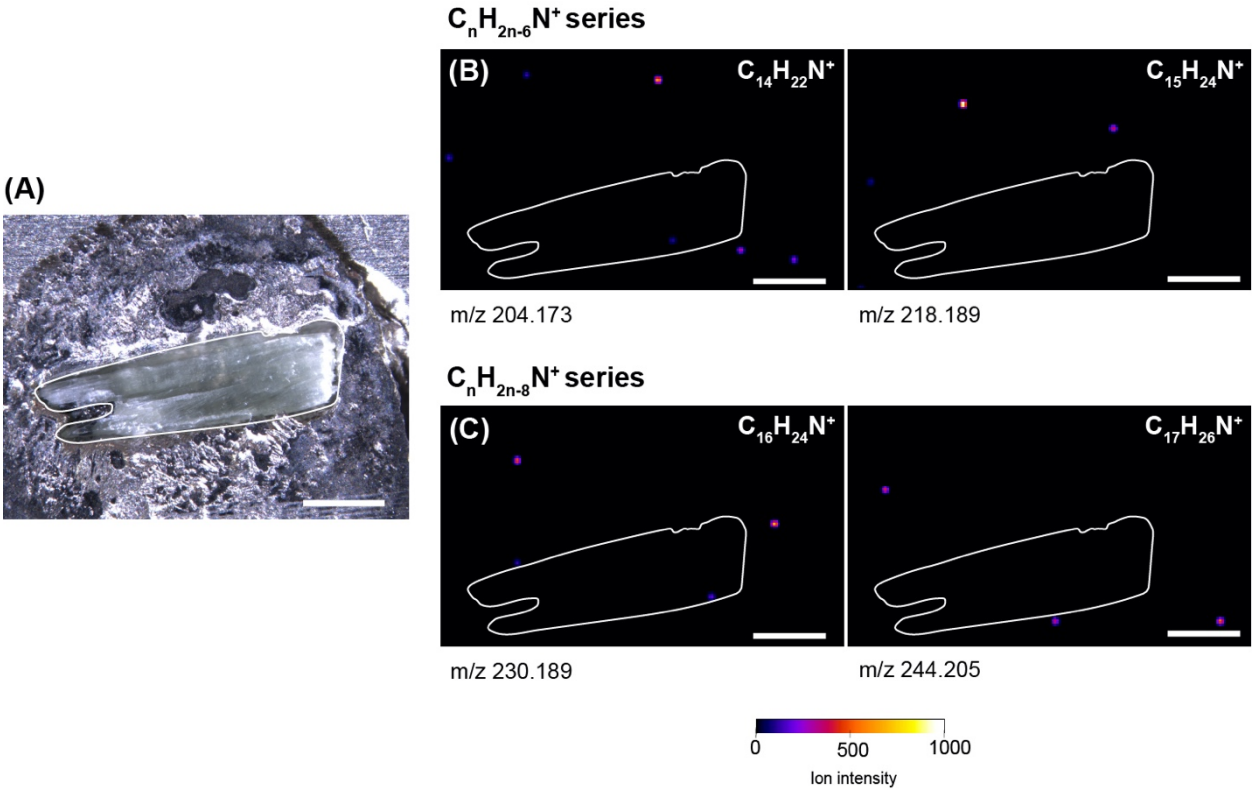

Fig. S8. Spatial distributions of organic molecules on the surface of an antigorite grain measured by DESI-HRMS. The measurement of the antigorite surface was performed as a blank for the A0080 sample shown in Fig. 7. (A) An optical image of an antigorite grain embedded in a soft alloy. (B) Maps of $C_nH_{2n-6}N^+$ series (n = 14, 15) and (C) $C_nH_{2n-8}N^+$ series (n = 16, 17) molecules. White outlines show the boundary between an antigorite grain and surrounding metal. The scale bar in the images is 500 μm.

Table S1. Carbon, nitrogen, hydrogen, oxygen, and sulfur contents (wt%) with their stable isotopic compositions of the Ryugu grains in the A0106 sample.

Ryugu A0106	Carbon (wt%)	$\delta^{13}C$ (‰ vs. VPDB)	Nitrogen (wt%)	$\delta^{15}N$ (‰ vs. Air)	weight C/N ratio
#1	3.69	-2.7	0.16	+39.1	23.8
#2	3.93	+1.4	0.17	+53.2	23.1
#3	3.68	-0.4	0.16	+36.7	23.7
Average (3 analyses)	**3.76±0.14**	**-0.58±2.0**	**0.16±0.01**	**+43.0±9.0**	**23.5±0.4**
	Hydrogen (wt%)	**δD (‰ vs. VSMOW)**	**Oxygen (wt%)***	**$\delta^{18}O$ (‰ vs. VSMOW)**	**weight O/H ratio**
#4	1.05	+240	12.5	+10.5	11.9
#5	1.15	+265	13.3	+12.8	11.5
#6	1.22	+250	13.0	+14.4	10.7
Average (3 analyses)	**1.14±0.09**	**+252±13**	**12. ±0.4**	**+12.6±2.0**	**11.4±0.6**
	Sulfur (wt%)	**$\delta^{34}S$ (‰ vs. VCDT)**			**weight C/S ratio**
#7	2.6	-1.1			-
#8	3.9	-2.4			-
#9	3.3	-5.6			-
Average (3 analyses)	**3.3±0.7**	**-3.0±2.3**			**1.15**

*Pyrolyzed oxygen released at 1400ºC under a helium gas flow.

Table S2. C, N and H contents (wt%) with their stable isotopic compositions of carbonaceous chondrites (CV, CR, CO, CM, and CI). All elemental abundances are wt%, the errors when known are indicated as 1 standard deviations for C and H wt% and δD and 2 standard deviations for N wt%, $\delta^{13}C$ and $\delta^{15}N$. $\delta^{13}C$ is vs. VPDB, $\delta^{15}N$ is vs. air, and δD is vs. VSMOW. Ryugu data is from Table S1. av.: Averaged value. n.d.: Not determined.

Sample	C (wt%)	$\delta^{13}C$ (‰)	N (wt%)	$\delta^{15}N$ (‰)	H (wt%)	δD (‰)	*References*
Ryugu A0106	**3.76±0.14**	**-0.58±2.0**	**0.16±0.01**	**43.0±9.0**	**1.14±0.09**	**252±13**	
CI							
Orgueil av.	3.10±0.50	-9.8±0.2	0.098±0.029	39.7±4.14	1.04±0.48	129.6±86.9	*79,81,83,84, 85,88,90*
Ivuna av.	3.50±0.20	-10.9±0.2	0.095±0.029	48.5±5.02	1.11±0.49	165.8±100.6	*13,79,81,85, 88*
Alais av.	3.90±0.80	-13.7±0.2	0.102±0.031		1.09±0.57	66.1±59.7	*13,85,90*
CM							
ALHA84034	1.74	2.2	0.061	16.1	1.40±0.00	-182.9±2.9	*88*
ALH 84042	1.68	0.8	0.060	15.3	1.35±0.01	-185.3±0.5	*88*
ALH 84044	1.71	2.3	0.061	15.3	1.33±0.01	-180.7±1.9	*88*
ALH 85013	1.73±0.05	-0.7±0.2	0.087±0.003	32.6±0.3	1.21±0.00	-137.6±0.5	*88*
Banten av.	1.87±0.13	-4.8	0.078	43.0	0.90±0.63	11.2±37.1	*13,82,85,87, 88*
Murchison av.	2.14±0.38	-4.9±3.88	0.103±0.027	45.8±6.85	0.97±0.14	-56.8±26.2	*81,83,85,86, 87,88,89,90*
ALHA81002	1.66	-9.4	0.069	13.6	1.30±0.01	-142.0±1.8	*88*
ALH 83100	1.9	-2.7	0.070	11.9	1.46±0.01	-201.1±0.5	*88*
ALH 84029	1.71	2.4	0.061	15.5	1.36±0.01	-184.1±2.5	*88*
DNG 06004	2.04	1.8	0.112	49.9	0.99±0.01	-3.4±1.1	*88*
DOM 08003	1.85	-0.5	0.095	41.1	1.46±0.01	-137.0±11.1	*88*
DOM 08013	1.92	-2.4	0.116	56.3	0.96±0.01	47.2±2.4	*88*
EET 96006	1.99	-1.8	0.124	39.2	1.28±0.00	-90.1±0.6	*88*
EET 96016	2.09	-1.4	0.121	44.8	1.25±0.01	-89.5±0.1	*88*
GRA 98074	2.04	0.7	0.116	49.4	1.11±0.03	-14.1±4.3	*88*
GRO 95566	1.93	0.5	0.110	55.7	1.10±0.02	-18.8±1.1	*88*
LAP 02239	1.91	3.7	0.101	45.6	1.03±0.02	-36.0±0.7	*88*
LAP 02333	2.1	1.0	0.141	35.4	1.13±0.01	-2.2±4.6	*88*
LAP 02336	2.02	-1.2	0.144	33.7	1.06±0.01	5.5±2.3	*88*
LAP 03718	2.03	-0.6	0.154	31.1	1.07±0.01	1.7±3.6	*88*
LAP 03785	1.81	-0.6	0.096	36.6	1.28±0.01	-123.6±0.8	*88*
LEW 85311	2.03	-3.1	0.156	33.1	0.91±0.04	119.4±2.9	*88*
LEW 85312	2.12	-0.8	0.171	37.5	0.95±0.02	126.3±4.1	*88*
LEW 87016	1.95	-1.8	0.124	48.1	1.13±0.01	-26.0±2.0	*88*
LEW 87022	1.88	1.6	0.093	29.9	1.20±0.01	-112.9±2.4	*88*
LEW 87148	1.81	-1.9	0.099	43.0	1.27±0.03	-102.2±4.5	*88*
LEW 88001	1.97	0.9	0.101	48.8	1.11±0.01	-50.2±0.0	*88*
LON 94102	2.06±0.05	-1.8	0.123±0.003	38.0±0.1	0.93±0.01	21.7±0.7	*88*
MAC 88101	1.73±0.01	1.2±0.1	0.097±0.004	51.6±1	1.20±0.00	35.0±5.1	*88*
MAC 88176	1.67	-3.0	0.093	22.4	1.20±0.02	-107.4±2.7	*88*
MCY 05230	2	1.5	0.110	47.3	0.98±0.01	-17.6±3.7	*88*
MET 00432	2.72±0.02	3.0±0.5	0.118±0.004	29.8±1	1.07±0.02	45.3±0.2	*88*
MET 01070	1.58	-9.0	0.087	-4.8	1.36±0.00	-220.3±0.0	*88*
Mighei av.	2.67±0.23	-10.8±1.45	0.095±0.011		1.11±0.18	-99.2±7.3	*79,81,85,88, 90*

Murray av.	2.24±0.60	-5.8±4.96		42.0±4.24	0.91±0.14	-22.7±43.4	*79,81,83,85, 88,90*
Nogoya av.	2.03±0.18	-9.6±2.97	0.064±0.008	14.7±1.47	1.28±0.26	-147.7±36.2	*13,85,88*
QUE 97990	2	-4.2	0.109	40.9	1.04±0.01	-22.2±1.0	*88*
QUE 99355	1.53±0.01	-8.4±0.1	0.077	15.3±0.3	1.13±0.00	-125.0±2.3	*88*
SCO 06014	1.34	-5.5	0.063	-2.8	1.33±0.01	-162.0±2.0	*88*
SCO 06043	1.45	-11.3	0.071	-3.6	1.39±0.00	-226.7±0.0	*88*
SCO 06043	1.23	-8.0	0.063	-6.0	1.34±0.03	-218.6±4.0	*88*
TIL 91722	2.04	0.7	0.121	56.3	0.90±0.01	53.7±0.7	*88*
Y-791198	2.43	-2.4	0.133	47.4	1.21±0.00	-8.9±1.0	*88*
Sayama	1.99	4.5	0.080		1.43	-172.0±3.0	*92*
Paris av.	2.16±0.73	-7.5	0.172		0.74±0.23	107.0±18.8	*90,91,92*
Boriskino	1.81	-7.7	0.052	16.0	0.89	-176.0	*13*
Cochabamba	2.03	-10.6	0.067	35.0	0.79	-63.0	*13*
Erakot	1.85	-9.3	0.070	43.0	0.80	-105.0	*13*
Pollen	3.22	-14.7	0.115	39.0	0.78	-80.0	*13*
Santa Cruz	1.98	-5.1	0.085	n.d.	0.50	3.0	*13*
Haripura	1.6	-3.7			0.81	-74.0	*79*
Nawapali	1.9	-10.0			1.00	-111.0	*79*
Santa Cruz	2.2	-4.3			0.93	-49.0	*79*
ALH 83100					1.60±0.03	-156.2±5.2	*85*
Y-791824					1.39±0	-129.9±3.1	*85*
EET 83334					1.51±0.01	-188.4±3.8	*85*
Pollen					1.52±0.32	-75.6±2.8	*85*
Y-791198					1.61±0.02	26.1±1.9	*85*
LEW 90500					1.73±0.01	-47.4±1.3	*85*
ALH 85004					0.36±0.09	23.1±19.4	*85*
BUC 10943	1.52	-7.6	0.095	15.0	1.22±0.004	-109.1±2.6	*89*
MIL l090073	0.72	-14.7	0.047	10.5	0.60±0.001	-136.0±0.5	*89*
Aguas Zarcas	2.13±0.04	-9.8±0.2	0.098±0.029	n.d.	0.87±0.05	-107.1±2.0	*90*
Jbilet Winselwan	1.54±0.03	-10.9±0.2	0.095±0.029	n.d.	0.47±0.03	-38.9±2.0	*90*
LON 94101	1.91±0.04	-13.7±0.2	0.102±0.031	n.d.	0.83±0.05	-154.6±2.0	*90*
Maribo	2.18±0.04	-5.5±0.2	0.114±0.034	n.d.	0.79±0.04	-37.9±2.0	*90*
Mukundpura	2.08±0.04	-3.9±0.2	0.086±0.086	n.d.	1.01±0.05	-158.2±2.0	*90*
CR							
Al Rais av.	2.59±0.19	-11.6±0.21	0.126±0.056	134.5± 29.19	1.11±0.38	646.8±80.4	*13,82,85,86, 88*
EET 92042	1.18	-4.9	0.091	178.7	0.42±0.01	752.5±14.9	*88*
EET 96268	1.03	-1.9	0.074	173.0	0.38±0.02	610.7±33.9	*88*
GRA 95229	1.09	0.0	0.078	178.2	0.42±0.02	654.6	*88*
GRO 95577	1.18	-9.2	0.061	182.8	1.29±0.03	266.4±4.5	*88*
LAP 2342	1.13	-1.9	0.088	162.8	0.40±0.02	691.5±12.8	*88*
LAP 4720	1.29	-1.2±0.2	0.100±0.004	166.1±1	0.38±0.02	763.1±9.1	*88*
MET 426	1	-3.3	0.068	179.8	0.36±0.01	612.4	*88*
PCA 91082	1.31	-2.2	0.101	177.1	0.58±0.02	576.9	*88*
QUE 99177	1.26	-7.3	0.088	184.1	0.47±0.03	662.7	*88*
Renazzo av.	1.64±0.53	-7.4±2.05	0.074±0.019	173.6±16.5	0.50±0.13	674.0±246.0	*81,83,84,85, 86,88*
EET 87770	1.42±0.07	-6.7±1.32	0.110±<0.01	184.0±2.6	0.48±0.08	367.0±32.0	*86*
Y-790112	1.29±0.04	-4.8±0.15	0.050±<0.01	178.0±5.1	0.77±0.02	422.0±21.6	*86*
Kaidun	3.34	-9.3	0.189	165.0	0.64	1045.0	*13*
EET 96286					0.60±0.08	282.0±140.9	*85*
EET 87770					0.47±0.08	366.6±16.5	*85*
Y-790112					0.77±0.03	421.8±21.6	*85*

CV							
Allende av.	0.41±0.16	-20.9±3.08	0.007±0.008	22.0	0.03±0.03	13.9±119.6	*14,83,84,85, 90*
Bali av.	0.69±0.15	-19.3±0.92	0.005	-10.0	0.05±0.01	-3.2±70.4	*13,85,87,90*
Kaba av.	1.21±0.19	-17.4±0.36	0.059	-22.9	0.16±0.08	44.9±111.9	*13,85,88,90*
Grosnaja av.	0.81±0.42	-22.7±1.48	0.022±0.017		0.29±0.21	-64.0±34.9	*13,85,90*
Leoville	0.77	-12.8	0.010	-24.0	0.093	-49.0	*13*
Mokoia av.	0.73±0.04	-17.8±0.42	0.007		0.08±0.02	239.6±54.5	*13,79,81*
Vigarano av.	0.50±0.71	-18.7	0.004±0.005		0.18±0.13	-35.3±34.3	*13,85,90*
ALH 84028					0.01±0.00	-45.9±22.6	*85*
CO							
ALHA77003 av.	0.28				0.15	15.8	*82,85,87*
DOM 03238	0.9	-11.9	0.035	-6.0	0.30±0.001	-73.1±0.4	*89*
ALHA77307	0.84	-7.1	0.025	-2.7	0.55±0.01	-48.2±4.4	*88*
Felix	0.64	-14.2	0.003	-22.0	0.02	-62.0	*13,79*
Kainsaz av.	0.39	-18.5	0.003	-30.0	0.05±0.04	56.9±137.3	*13,85*
Lancé av.	0.40±0.08	-16.4±0.92	0.004	13.0	0.14±0.13	-98.2±15.5	*13,79,85*
Warrenton av.	0.25	-19.3	0.003		0.05±0.04	-115.2±45.0	*13,85*
Y-791717					0.34±0.00	-49.8±2.3	*85*
FRO 95002					0.14±0.00	-70.6±0.8	*85*
ALH 82101					0.11±0.00	-78.3±5.3	*85*
DOM 08006	1.19	-5.0	0.019	6.5	0.44±0.005	4.7±4.8	*89*
DOM 08004	0.91	-11.3	0.031	-7.9	0.33±0.001	-89.8±3.8	*89*
DOM 10104	0.88	-11.7	0.072	-5.9	0.40±0.002	-98.7±1.3	*89*
MIL 03377	0.64	-7.3	0.032	-5.5	0.39±0.02	-92.9±0.3	*89*
MIL 05013	0.65	-7.1	0.100	-7.2	0.29±0.03	-73.7±0.2	*89*
MIL 05024	0.64	-7.6	0.032	-7.8	0.35±0.001	-89.7±3.2	*89*
MIL 07182	0.66	-7.0	0.027	-8.5	0.33±0.004	-85.5±1.2	*89*
MIL 07193	0.63	-7.6	0.030	-8.4	0.65±0.01	-85.8±3.8	*89*
MIL 07709	0.62	-7.0	0.021	-8.1	0.31±0.002	-85.4±0.3	*89*
MIL 090010	0.69	-6.5	0.016	-4.9	0.37±0.001	-94.0±0.1	*89*
MIL 090038	0.64	-7.2	0.035	-3.3	0.34±0.01	-83.9±3.1	*89*

Table S3. **Comparison of amino acid and amine abundances as detected by 3D-HPLC/FD and LC-FD/HRMS in hot water extracts of Ryugu sample A0106 and the CI carbonaceous chondrite Orgueil.** n.t.: Not targeted by 3D-HPLC/FD. n.d.: Not determined. For Ryugu at KU, the concentration was determined by single analysis. For Ryugu at GSFC, reported uncertainties are based on the standard deviation (σ_x) of the average value of multiple individual measurement (N), where $\delta_x=\sigma_x(N)^{-1/2}$. The Orgueil data are from (*23, 31*).

Amino Acid	Ryugu (A0106) Hydrolyzed (KU) nmol g^{-1}	Ryugu (A0106) Hydrolyzed (GSFC) nmol g^{-1}	Orgueil (CI) Hydrolyzed (*23*) nmol g^{-1}
D-Aspartic acid	n.t.	<0.06	0.41±0.23
L-Aspartic acid	n.t.	0.018±0.010	0.41±0.21
D-Glutamic acid	n.t.	<0.03	0.32±0.11
L-Glutamic acid	n.t.	<0.03	0.56±0.15
D-Serine	n.t.	0.056±0.014	<0.01
L-Serine	n.t.	0.182±0.034	<0.01
Glycine	5.6	0.456±0.053	11.5±6.0
β-Alanine	n.t.	3.29±0.14	30.6±7.6
D-Alanine	0.72	0.0246±0.0062	0.90±0.19
L-Alanine	0.80	<0.44	1.1±0.25
ɣ-Amino-*n*-butyric acid	n.t.	3.51±0.18	2.7±1.3
D-β-Amino-isobutyric acid	n.t.	0.201±0.014	n.d.*†
L-β-Amino-isobutyric acid	n.t.	0.170±0.018	
D-β-Amino-*n*-butyric acid	n.t.	0.324±0.011‡	2.1±1.1
L-β-Amino-3-butyric acid	n.t.	0.322±0.010‡	1.8±0.6
α-Amino-isobutyric acid	n.t.	0.383±0.023	3.3±1.4
D-α-Amino-*n*-butyric acid	0.11	<0.01	0.69±0.48†
L-α-Amino-*n*-butyric acid	0.11	<0.01	
D-Valine	0.026	<0.07	0.19±0.05
L-Valine	0.056	<0.06	0.48±0.02
D-Norvaline	0.017	<0.04‡	0.23±0.02†
L-Norvaline	0.017	<0.04‡	
D-Isovaline	0.053	<0.05	0.31±0.03
L-Isovaline	0.047	<0.05	0.42±0.02
R,S-β-Amino-*n*-pentanoic acid	n.t.	<0.14	1.6±0.1
δ-Amino-*n*-valeric acid	n.t.	1.160±0.089‡	1.2±0.2
D,L-3-Amino-2-methylbutyric acid	n.t.	0.18	0.55±0.03
3-Amino-3-methylbutyric acid	n.t.	0.29	<0.26
3-Amino-2,2-dimethylbutyric acid	n.t.	0.0555±0.0021‡	0.59±0.03
R,S-3-Amino-2-ethylpropanoic acid	n.t.	1.4§	1.5±0.1
D,L-ɣ-Amino-*n*-valeric acid	n.t.	0.86§	2.4±0.2
D,L-4-Amino-2-methylbutyric acid	n.t.	<0.17	1.5±0.1
D,L-4-Amino-3-methylbutyric acid	n.t.	0.18§	2.8±0.1

Amine	Ryugu (A0106) Unhydrolyzed (GSFC) nmol g^{-1}	Orgueil (CI) Unhydrolyzed (*31*) nmol g^{-1}
Methylamine	23.79±0.52	331.5±0.2
Ethylamine	11.37±0.27	27.3±2.4
n-Propylamine	0.0521±0.0058	4.8±0.04
Isopropylamine	0.59±0.026	5.1±0.1
Butylamines	<0.1	7.6±0.5

[*]Analyte was reported as detected but not quantified in (*23*), in part, because a lack of optically pure standards prevented proper quantification of the analyte's two enantiomers.
[†]Sum of both enantiomers, which could not be separated under chromatographic conditions.
[‡]Quantification of analytes was performed using Orbitrap MS due to interfering, optically fluorescent species.
[§]Analyte was tentatively detected, but not quantified. Therefore, an upper limit estimate is provided for the analyte instead.

Table S4. Blank subtracted abundances of carboxylic acids in the hot-water extract of Ryugu (A0106) and the highly aqueously altered CM-type carbonaceous chondrite ALH 83100 (*36*)**.** n.a.: Not analyzed. Values are the average of three measurements with errors shown as standard deviations (σ_x) of the average value of multiple individual measurement (N), where where $\delta_x=\sigma_x(N)^{-1/2}$.

Monocarboxylic Acids	Ryugu (A0106)* (nmol g^{-1})	ALH 83100 (CM) (*36*) (nmol g^{-1})
Formic acid	9466±103	n.a.†
Acetic acid	5708±1536	4455±383
Propanoic acid	< 0.1	281±24
Isobutyric acid	< 0.1	< 0.7
2,2-Dimethylpropanoic acid	< 0.1	< 0.01
Butyric acid	< 0.1	11±2
2-Methylbutyric acid	< 0.1	< 0.7
Isopentanoic acid	< 0.1	< 0.7
2,2-Dimethylbutyric acid	< 0.1	< 0.01
3,3-Dimethylbutyric acid	< 0.1	< 0.01
Pentanoic acid	< 0.1	< 0.7
2-Ethylbutyric acid/2-Methylpentanoic acid	< 0.1	< 0.01
3-Methylpentanoic acid	< 0.1	< 0.7
4-Methylpentanoic acid	< 0.1	< 0.7
Hexanoic acid	< 0.1	< 0.01
Benzoic acid	< 0.1	< 0.01
Total carboxylic acids	15174±1639	4747±410†

*Compounds identified by comparison of elution time and mass spectra to that of standards.
†Formic acid was detected but could not be isolated.

Table S5. Relative abundance of $C_nH_{2n-5}N$ molecules in the MeOH extracts of Ryugu A0106 sample and Murchison meteorite for comparison. Peak areas are in arbitrary unit derived from ion intensity × time. n.d.: Not detected. Chromatographic data is provided as Data S13 at (*74*).

Formula	Theoretical mass (Da)	$[M+H]^+$ (Da)	A0106 Peak area ($\times 10^6$)	A0106 Peak Ratio vs. C_{17}=100	Murchison Peak area ($\times 10^6$)	Murchison Peak Ratio vs. C_{11}=100
C_5H_5N	79.0422	80.0495	58.8	22.1	32.0	0.64
C_6H_7N	93.0578	94.0651	29.9	11.2	21.2	0.43
C_7H_9N	107.0735	108.0808	58.7	22.0	424	8.52
$C_8H_{11}N$	121.0891	122.0964	72.0	27.0	1668	33.5
$C_9H_{13}N$	135.1048	136.1121	68.5	25.7	3033	60.9
$C_{10}H_{15}N$	149.1204	150.1277	86.1	32.3	4058	81.5
$C_{11}H_{17}N$	163.1361	164.1434	109.9	41.3	4977	100
$C_{12}H_{19}N$	177.1517	178.1590	132.1	46.7	4392	88.3
$C_{13}H_{21}N$	191.1674	192.1747	132.2	49.6	4064	81.7
$C_{14}H_{23}N$	205.1830	206.1903	179.5	67.4	2988	60.0
$C_{15}H_{25}N$	219.1987	220.2060	210.3	79.0	1971	39.6
$C_{16}H_{27}N$	233.2143	234.2216	254.8	95.7	1146	23.0
$C_{17}H_{29}N$	247.2300	248.2373	266.3	100	613	12.3
$C_{18}H_{31}N$	261.2456	262.2529	264.0	99.1	331	6.65
$C_{19}H_{33}N$	275.2613	276.2686	228.3	85.7	188	3.78
$C_{20}H_{35}N$	289.2769	290.2842	173.7	65.2	95.3	1.91
$C_{21}H_{37}N$	303.2926	304.2999	136.8	51.4	58.0	1.17
$C_{22}H_{39}N$	317.3082	318.3155	101.8	38.2	30.5	0.61
$C_{23}H_{41}N$	331.3239	332.3312	71.2	26.7	19.9	0.40
$C_{24}H_{43}N$	345.3395	346.3468	53.3	20.0	11.9	0.24
$C_{25}H_{45}N$	359.3552	360.3625	36.3	13.6	3.94	0.079
$C_{26}H_{47}N$	373.3708	374.3781	24.6	9.24	1.91	0.038
$C_{27}H_{49}N$	387.3865	388.3938	16.0	6.01	0.226	0.0045
$C_{28}H_{51}N$	401.4021	402.4094	10.6	4.20	0.0500	0.0010
$C_{29}H_{53}N$	415.4178	416.4251	6.92	3.98	n.d.	0.00
$C_{30}H_{55}N$	429.4334	430.4407	2.91	1.09	n.d.	0.00
$C_{31}H_{57}N$	443.4491	444.4564	1.62	0.61	n.d.	0.00
$C_{32}H_{59}N$	457.4647	458.4720	0.497	0.19	n.d.	0.00
$C_{33}H_{61}N$	471.4804	472.4877	0.161	0.060	n.d.	0.00